A Study of Two Spectroscopic Binary Systems

by

Joanne Marie Rosvick
B.Sc., University of Alberta, 1987

A THESIS SUBMITTED IN PARTIAL FULFILLMENT
OF THE REQUIREMENTS FOR THE DEGREE OF
MASTER OF SCIENCE
in the Department
of
Physics and Astronomy

We accept this thesis as conforming
to the required standard

[redacted]
Supervisor: Dr. C. D. Scarfe

[redacted]
Dr. A. C. Gower

[redacted]
Dr. M. B. Hocking

[redacted]
Mr. J. M. Fletcher

Abstract

Supervisor: Dr. C. D. Scarfe

Strömgren *uvby* photometry of the spectroscopic–visual triple system 20 Leonis was obtained at the San Diego State University's Mount Laguna Observatory. The δ Scuti visual component was found to have only one period of 0.0826 days, although another may be present in the data. The close pair was found to undergo grazing eclipses from which an inclination of 75 $\pm$ 1 degrees was tentatively determined. The close pair's radial velocities obtained from the Dominion Astrophysical Observatory's 48 inch telescope were combined with Fekel and Bopp's (1977) velocities and new orbital elements were calculated. Spectroscopic observations of the visual component also showed that there has been an observable change in the system since 1977.

High dispersion (2.4 Å/mm) photographic spectra of the composite spectrum binary α Equulei were reduced using the ARCTURUS measuring machine for the G component's spectrum, and a radial velocity cross-correlation package within IRAF for the A component's spectrum, to obtain new orbital elements and investigate the awkward possibility that the evolved G star is less massive than the main sequence A star. It was found that subtraction of the G star's contribution to the composite spectrum before cross–correlation gave consistently better results than cross–correlation alone. New orbital elements were calculated and it was determined that the mass ratio M_G/M_A is equal to 1.149 $\pm$ 0.046. Thus the mass of the evolved

star is greater than that of its companion as expected from evolutionary considerations.

Examiners:

[redacted]

Supervisor: Dr. C. D. Scarfe

[redacted]

Dr. A. C. Gower

[redacted]

Dr. M. B. Hocking

[redacted]

Mr. J. M. Fletcher

Acknowledgements

With the completion of any large piece of work, there are those along the way whose assistance made it all possible. I have several people to thank for helping me to my goal. First and foremost, I'd like to thank Colin Scarfe for encouraging me to choose the topic and for sending me to San Diego to obtain the observations. I appreciated his patience and helpful suggestions, as well as lively discussions which were not always on the topic of this work!

I would also like to acknowledge all those at Mt. Laguna: Ron Angione for welcoming me to the Observatory, Paul Etzel for his assistance and good humour, and other students and visiting astronomers who helped to make it a very enjoyable and educational experience.

For the people at UVIC: thanks go to Russ Robb, whose plethora of computer programs and vast knowlege of photometry, as well as his sense of humour made this undertaking much easier. Thanks also to Dave Barlow for the use of other very useful computer programs. I am grateful to the other grad students here at UVIC whose friendship and support kept me going through the rough stuff.

Since half of this work took place at the DAO, I would like to thank all those up there who helped me. However, special mentions must go to Eileen Friel and Wes Fisher. Eileen's patience and understanding while I was learning IRAF was greatly appreciated, and Wes' help with the PDS machine and IRAF, and his light–hearted approach to things made my first few days up there much less intimidating.

On the home front, I am very grateful to my family and my husband Myron for their emotional support and encouragement, and for trying to understand my explanations of the how, what and why of binary stars.

Contents

List of Figures

List of Tables

Chapter 1

Introduction

Binary stars, or stars which describe stable orbits about each other due to their mutual gravitational attraction, have been observed for hundreds of years, but the first actual measurement of a double star was not recorded until the late eighteenth century. Sir William Herschel recorded this measurement in a catalogue in 1776, and three years later began actively searching for these stars. In 1802, he published a paper which introduced the term "binary star", and spent the next thirty or so years of his life composing catalogues of binaries (Aitken, 1935).

It has now been determined that at least fifty percent of all main sequence stars are members of spectroscopic binary systems. These systems consist of two close stars whose orbital motion is apparent from shifts in the stars' spectra. Some of these spectroscopic systems are eclipsing binaries, or binaries in which the stars periodically pass in front of each other, causing a diminution of the total light of the system. These types of systems are important to astronomical research because they allow the determination of fundamental physical properties of the stars and their orbits. The next sections of this chapter will briefly introduce these classes of binaries; detailed descriptions as well as solution methods will appear in later chapters.

1.1 Spectroscopic Binary Systems

As was mentioned previously, binaries consist of two stars which move in closed orbits due to mutual gravitational attraction. If the two stars are separated widely enough that both may be seen through a telescope, they form a visual binary system and the orbital motion may be observed directly. Of course, widely separated stars imply very long periods of revolution, so only partial orbits of these binaries may be obtained in any single observer's lifetime.

The binary systems for which orbital solutions may be obtained more readily are the spectroscopic binary systems. The stars in these systems are so close together that they cannot be resolved by a telescope, but may be analysed by examining the spectra and measuring the shifts in wavelengths of the spectral lines. From these shifts, the radial (or line of sight) velocities may be calculated at various phases of the orbital cycle, resulting in a radial velocity curve which may be used to calculate the orbital elements of the system. These systems are more easily detected if the amplitude of the velocity variation is large, which normally occurs in the more massive systems, and those of short period.

The spectrograms of these systems may show one or two sets of lines. Systems pertaining to the latter case are called double–lined spectroscopic binaries, and are very useful since the radial velocities of both stars, orbital elements of the system and lower limits to the stars' masses may be determined. Single–lined spectroscopic binaries are characterized by only one set of lines, since one star is faint compared to the other and its lines are obliterated by the latter's spectrum. These systems are detected by the radial velocity variation of the brighter star, and are not as useful as the double–lined case, since only one component of the radial velocity curve may be used

to determine the orbital elements; the amplitude of the velocity variation for the fainter star remains unknown and the determination of lower limits of the stars' masses is impossible.

1.2 Composite Spectrum Binaries

There exist double–lined spectra for which it is obvious that the two stars are of different spectral types. These systems are the composite spectrum binaries, and were first detected in 1891 by Pickering. Some work was done on this group of stars in the few decades which followed (Shajn, 1926 for example), but the first real study was performed by Hynek (1938), who completed a survey of 566 composite spectrum binaries, some of which were later reclassified. Recent analyses have been performed by Griffin (1986), using precise observations and sophisticated reduction techniques.

Before an explanation of the problems associated with composite spectra is undertaken, a brief description of the Morgan–Keenan and Harvard Systems of spectral classification is necessary. The Harvard scheme is based on the relative strengths of spectral features, and recognises seven main spectral types (which are divided further into finer regions). These classes, in order of decreasing temperature, are O, B, A, F, G, K and M. The Morgan–Keenan luminosity scheme orders stellar spectra of the same temperature by the relative intensity of certain spectral lines. The six luminosity classes, in order of decreasing luminosity, are designated by Ia, Ib, II, III, IV and V and are illustrated in Figure 1.1.

There are many problems associated with the analysis of composite spectrum binaries, and these problems often lead to difficulties in not only classifying the spectra, but in determining accurate radial velocities. In most composite spectra, a cool, luminous, evolved primary star is paired with an

Figure 1.1: The Morgan–Keenan luminosity classes, from Zeilik and Smith (1987), p.239.

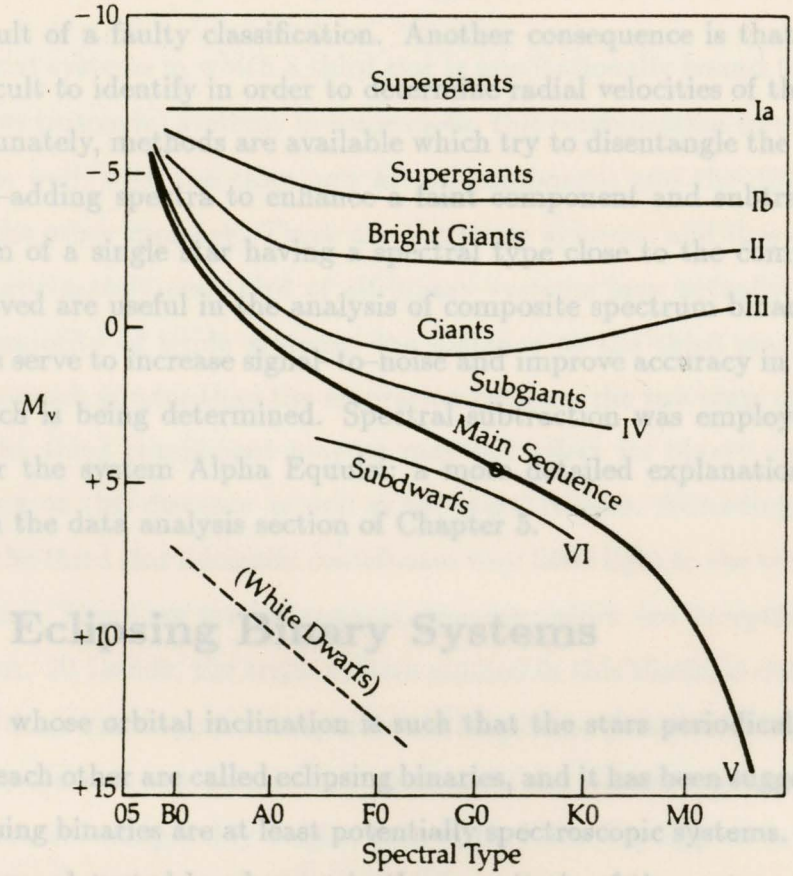

Notes: Class *VI* arises because the subdwarfs are metal-deficient stars; decreased line blanketing causes the stars to appear to be earlier in spectral type than they actually are. M_v is absolute visual magnitude.

unevolved or slightly evolved secondary star, usually of spectral type B or A. If the difference in magnitude is large, the spectrum of the brighter star will dominate that of the fainter component. Even if the magnitude difference is not great, spectral classification of the primary star may be difficult due to contamination from the secondary, and vice versa. One consequence is that an incorrect determination of spectroscopic absolute magnitudes may arise as a result of a faulty classification. Another consequence is that the lines are difficult to identify in order to determine radial velocities of the stars.

Fortunately, methods are available which try to disentangle the two spectra. Co–adding spectra to enhance a faint component and subtracting the spectrum of a single star having a spectral type close to the component to be removed are useful in the analysis of composite spectrum binaries. Both methods serve to increase signal–to–noise and improve accuracy in the quantity which is being determined. Spectral subtraction was employed in this work for the system Alpha Equulei; a more detailed explanation may be found in the data analysis section of Chapter 5.

1.3 Eclipsing Binary Systems

Systems whose orbital inclination is such that the stars periodically pass in front of each other are called eclipsing binaries, and it has been suggested that all eclipsing binaries are at least potentially spectroscopic systems. Eclipsing binaries are detected by changes in the magnitude of the system, and their discovery depends on the fraction of time spent in eclipse as well as the depth of the eclipse.

Eclipsing binary systems are analysed using a light curve, which is a plot of the change in the light received from the system versus orbital phase. The light curve enables the astronomer to determine the fraction of light

from each star, the orbital inclination, the period and the radii of the two stars in terms of the orbit radius. When these results are combined with the spectroscopic results, the stars' masses and sizes, as well as the absolute size of the orbit, may be computed.

1.4 Triple Systems

There exist systems in which a third star is gravitationally bound to a binary (often spectroscopic) system. In some cases, this configuration forms a visual binary as well, with the close pair as one component and the distant third star as the other member. These are the triple systems, and it is estimated that approximately one third of all binary systems may actually be triple. In the majority of triple systems, the distance to the third star from the binary is much greater than the separation between the two stars of the close pair. The third component may or may not affect its binary companion, depending on this distance as well as the stars' masses. According to Kopal (1959), the third star normally contributes very little light to the total light of the system. There are several systems, however, which are exceptions to this statement. 20 Leonis, the triple system studied in this thesis, is one example since all three stars appear comparable in brightness (Fekel and Bopp, 1977).

Triple systems are detected by examining the system's spectrum. If all three stars are comparably bright, then triple lines may appear in the spectrum. This is the case with 20 Leonis. Even if the third star is too faint to allow detection by its lines in the system's spectrum, its mass may affect the close pair's orbit, and lead to changes in the orbital elements.

The relative inclination of the orbits do not appear to show a preference for co–planarity (Worley, 1967), but there seems to be disagreement as to whether or not triple systems are co–revolving. Batten (1973), and Kopal

(1959) both state that the senses of revolution of the close pair and wide pair are not necessarily the same, but Heintz (1978) claims that the sub–system and the main system usually co–revolve. Since there are so few systems for which both orbits are solved, this question probably will remain unsettled for some time.

1.5 δ Scuti Variable Stars

A δ Scuti star is a pulsating variable star of spectral type A or F, having a period of pulsation less than about 0.25 days, with a mass equal to, or greater than, about 1.3 solar masses (Breger, 1975), and luminosity amplitudes between about 0.02 and 0.4 magnitudes. The light curves are generally sinusoidal, but may show small bumps or other irregularities. It is speculated that the longer the period of pulsation, the larger the amplitude of variation.

One of the most distinguishing characteristics of δ Scuti stars is the instability of the light curve. This is probably due to the pulsation mechanism of these stars. The ionisation of helium in the outer layers of the star gives rise to radial pulsations, and a superposition of two or more modes often results in beat amplitudes and periods. This causes apparent variations of the period, amplitude and shape of the light curve, and in extreme cases, a complete temporary absence of the luminosity variation (Frolov, 1975).

1.6 Objectives of Study

The first system studied in this work was 20 Leonis, a triple system consisting of three nearly identical stars of spectral type *A*m. Fekel and Bopp (1977, hereafter FB) obtained a radial velocity curve for the close pair as well as velocities for the visual companion. They found that the orbit of the spectroscopic system is nearly circular, and the δ Scuti star is the third star in the

system. They also suggested the possibility of eclipses. Barnes, Fekel and Moffett (1977) obtained five photometric observations of 20 Leonis, put loose limits on the eclipse depth and inclination of the system, and recommended that the system be observed with the intention to model eclipses (if present) and thus determine the masses of two *A*m stars. Elliott (1974) studied the δ Scuti star in order to obtain the period and amplitude of the variation. He found values of 0.0818 days, and 0.02 magnitudes, and no evidence for beats. I observed this system in order to

- verify Elliott's value of the δ Scuti period, and observe the variation of the period and amplitude,
- try to find multiple periods for the δ Scuti component,
- determine whether or not the spectroscopic sub-system undergoes eclipses and, if possible, model those eclipses,
- obtain more coverage of the radial velocity curve, and calculate new orbital elements.

The composite spectrum binary α Equulei was also studied. This system consists of a main sequence *A*–type star and a *G*–type giant, and was first studied in detail by Deutsch (1954). He constructed a radial velocity curve based on six observations for each component, and found the mass ratio ($\equiv M_A/M_G$) to be 3.89, but did caution against accepting the orbital elements as anything more than tentative. A more complete radial velocity curve by Stickland (1976) lowered the mass ratio to 1.25, but both these values imply that the less evolved star is more massive than the more evolved star. Since massive stars evolve more quickly, one would expect that the *G* star must have been initially more massive, and that mass transfer from the *G* star to

the *A* star must have occurred in the past. However, since the period is almost 100 days, mass transfer could not have occurred easily in this relatively wide system.

In an attempt to clear up the confusion, Pike (1978) used Stickland's data and the method of cross-correlation to obtain radial velocities. He found a mass ratio of 0.80 ± 0.05 but the velocity curve still showed a great deal of scatter (rms deviations from the fitted curve are 1.3 and 2.7 km/s for the *G* star and *A* star, respectively). It was this author's hope that by using better data and sophisticated reduction techniques, a new radial velocity curve could be constructed, new orbital elements could be calculated and the (possible) mass ratio problem could be solved.

Chapter 2

Spectroscopic and Eclipsing Binaries

This chapter will present the basic theory of and solution methods for spectroscopic and eclipsing binaries. Only brief outlines will be given here; the reader is referred to Batten (1973), Heintz (1978) and Kopal (1959) for more detailed discussions.

2.1 Spectroscopic Binaries

2.1.1 Orbital Elements

The quantities which describe the orbit of a binary are known as the orbital elements (see Figure 2.1). The orbital period P is one of the first quantities to be determined from the radial velocity curve, and has come to be regarded as an element since it is required to complete the knowledge about the system. The inclination i is the angle between the orbital plane and the plane of the sky (the plane perpendicular to the line of sight). There are two nodes which differ by 180°; the ascending node (labelled N on Figure 2.1) is the point of intersection between the orbit of the star and the plane of the sky, where the star crosses the plane of the sky moving away from the sun. NN designates

Figure 2.1: Illustration of the orbital elements of a binary star. Based on Figure 1.3 of Batten (1973).

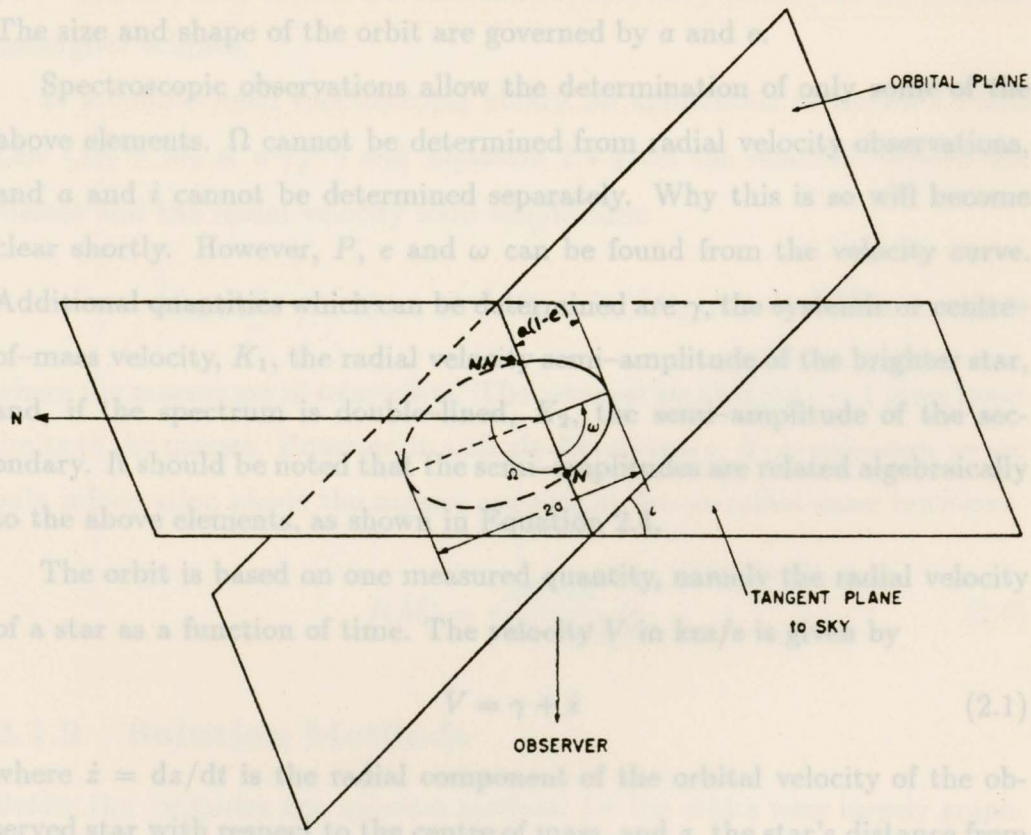

the descending node, and Ω is the position angle of the line of nodes. This angle is measured from north through east, in the plane of the sky. The longitude of periastron (ω) is the angle between the ascending node and the point at which the two stars are the closest together in the orbit, measured in the direction of motion. The time of periastron passage is denoted by T. The major semiaxis is a, while the eccentricity of the orbit is e. These quantities describe fully the orbit: the angles i and Ω define the orientation of the orbital plane, while ω gives the orientation of the orbit in its plane. The size and shape of the orbit are governed by a and e.

Spectroscopic observations allow the determination of only some of the above elements. Ω cannot be determined from radial velocity observations, and a and i cannot be determined separately. Why this is so will become clear shortly. However, P, e and ω can be found from the velocity curve. Additional quantities which can be determined are γ, the systemic or centre–of–mass velocity, K_1, the radial velocity semi–amplitude of the brighter star, and, if the spectrum is double–lined, K_2, the semi–amplitude of the secondary. It should be noted that the semi–amplitudes are related algebraically to the above elements, as shown in Equation 2.4.

The orbit is based on one measured quantity, namely the radial velocity of a star as a function of time. The velocity V in km/s is given by

$$V = \gamma + \dot{z} \tag{2.1}$$

where $\dot{z} = \mathrm{d}z/\mathrm{d}t$ is the radial component of the orbital velocity of the observed star with respect to the centre of mass, and z, the star's distance from the plane of the sky, is given by

$$z = r \sin(\nu + \omega) \sin i. \tag{2.2}$$

r is the radius vector and ν is the true anomaly. Differentiating Equation 2.2 with respect to time gives (after some algebra) the general radial velocity

equation which applies to either component:

$$V = \gamma + K[\cos(\nu + \omega) + e\cos\omega] \tag{2.3}$$

where

$$K = \frac{2\pi a \sin i}{86400P(1-e^2)^{1/2}}, \tag{2.4}$$

with K in km/s, P in days and a in km. This is the only place where a and i appear; they cannot be determined separately unless the system also undergoes eclipses.

In a double–lined spectroscopic binary, an application of Kepler's Third Law ($M_1 + M_2 \propto a^3/P^2$) and Equation 2.4 gives the relation between the masses and the radial velocity semi–amplitudes:

$$M_{1,2}\sin^3 i = 1.036 \times 10^{-7}(K_1 + K_2)^2 K_{2,1} P(1-e^2)^{3/2} \tag{2.5}$$

where the masses are in solar units. The assumption that $\sin i = 1$ gives lower limits to the masses. However, in a single–lined binary, K_2 is unknown, so the only information about the masses appears in the so–called mass function:

$$f(M) = \frac{M_2^3 \sin^3 i}{(M_1 + M_2)^2}. \tag{2.6}$$

2.1.2 Solution Methods

Before the computer era, solution methods for the orbits were largely graphical. The most widely used of these is the Lehmann-Filhés method (1894),

Figure 2.2: Illustration of quantities in the Lehmann–Filhés method. From Heintz (1978), p. 84.

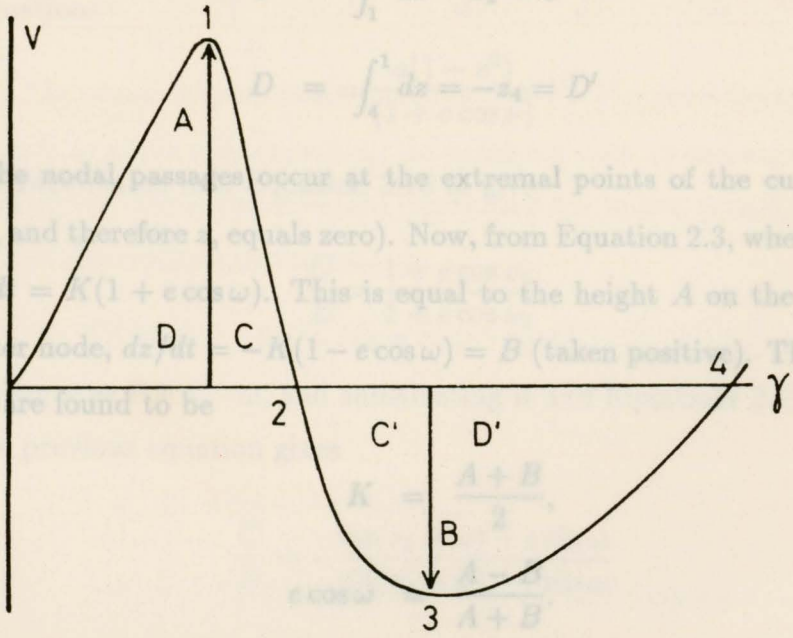

and is applied to the velocity curve of each component (Figure 2.2) as follows. The velocity integral over a closed path is equal to zero:

$$\int_0^P \dot{z}dt = \int_0^P dz = 0. \tag{2.7}$$

The areas above and below the γ axis are equal, hence γ is known. Note also that the areas C and C' are equal, as are D and D':

$$C = \int_1^2 dz = z_2 = C' \tag{2.8}$$

$$D = \int_4^1 dz = -z_4 = D' \tag{2.9}$$

since the nodal passages occur at the extremal points of the curve (where $(\nu+\omega)$, and therefore z, equals zero). Now, from Equation 2.3, when $(\nu+\omega) = 0$, $dz/dt = K(1 + e\cos\omega)$. This is equal to the height A on the curve. At the other node, $dz/dt = -K(1 - e\cos\omega) = B$ (taken positive). Thus, K and $e\cos\omega$ are found to be

$$K = \frac{A+B}{2}, \tag{2.10}$$

$$e\cos\omega = \frac{A-B}{A+B}. \tag{2.11}$$

A second equation is now needed to allow the separate determinations of e and ω. The expression for dz/dt in Equation 2.3 and the fact that $dz/dt = 0$ at points 2 and 4 give

$$\cos(\nu_2+\omega) = \cos(\nu_4+\omega) \tag{2.12}$$

$$= -e\cos\omega. \tag{2.13}$$

This and Equation 2.11 give

$$\sin(\nu_2+\omega) = -\sin(\nu_4+\omega) \tag{2.14}$$

$$= \pm 2\sqrt{AB}/(A+B). \tag{2.15}$$

It is conventional to take $\sin(\nu_2 + \omega)$ to be positive, since this corresponds to the point on the true orbit for which z has its maximum positive value. Now, from Equations 2.2 and 2.14,

$$\frac{C}{D} = \frac{r_2}{r_4}. \tag{2.16}$$

The equation

$$\mathbf{r} = \frac{a(1-e^2)}{(1+e\cos\nu)} \tag{2.17}$$

may be substituted into Equation 2.16 to give

$$\frac{C}{D} = \frac{1+e\cos\nu_4}{1+e\cos\nu_2}. \tag{2.18}$$

Expanding ν as $\nu + \omega - \omega$, and substituting it and Equations 2.12 and 2.14 into the previous equation gives

$$\frac{C}{D} = -\frac{\sin(\nu_2+\omega) - e\sin\omega}{\sin(\nu_4+\omega) - e\sin\omega} \tag{2.19}$$

from which it follows that

$$e\sin\omega = \frac{2\sqrt{AB}}{A+B}\frac{D-C}{D+C}. \tag{2.20}$$

The time of periastron passage T follows from the fact that at this point, $\nu = 0$ and therefore

$$\frac{dz}{dt} = K(1+e)\cos\omega. \tag{2.21}$$

The semi-amplitude K is found from $K = \frac{1}{2}(A+B)$.

Graphical methods are often used to obtain a set of preliminary elements which are then corrected by use of least–squares. While the velocity equation is not linear in the elements (the reason why a least squares solution could not be applied in the first place), the equation which is obtained by differentiating Equation 2.3 with respect to the elements *is* linear in the corrections (to first order):

$$\delta V = \frac{dV}{d\gamma}\delta\gamma + \frac{dV}{dK}\delta K + \frac{dV}{de}\delta e + \frac{dV}{d\omega}\delta\omega + \frac{dV}{dT}\delta T + \frac{dV}{dn}\delta n \qquad (2.22)$$

where n, the mean daily motion, is equal to $2\pi/P$. The general velocity equation as well as applicable ephemeris formulae are used to find expressions for the derivatives. Thus, the equation expressing the radial velocity correction in terms of the element corrections is

$$\delta V = \delta\gamma + a\delta K + b\delta e + c\delta\omega + d[n\delta T - (t-T)\delta n] \qquad (2.23)$$

where

$$a = e\cos\omega + \cos(\nu+\omega) \qquad (2.24)$$

$$b = K[\cos\omega - \frac{\sin\nu\sin(\nu+\omega)}{1-e^2}(2+e\cos\nu)] \qquad (2.25)$$

$$c = -K[e\sin\omega + \sin(\nu+\omega)] \qquad (2.26)$$

$$d = K\sin(\nu+\omega)\frac{(1+e\cos\omega)^2}{(1-e^2)^{3/2}}. \qquad (2.27)$$

If the eccentricity of the orbit is close to zero, the radial velocity curves are nearly sinusoidal, T and ω are undefined and c approaches $-d$, resulting in two identical columns in the solution matrix. Thus, an alternative approach (the method of Sterne (1941)) must be used. Only four preliminary elements are determined: γ, K, T_0 (the time of nodal passage) and P. The calculated

velocities are given by

$$V = \gamma + K \cos L \tag{2.28}$$

where $L = n(t - T_0)$ is the mean longitude measured from T_0. The corrected elements are found from the equation

$$\begin{aligned} dV &= d\gamma + \cos L dK + Ke \cos\omega \cos 2L + Ke \sin\omega \sin 2L + \\ &\quad Kn \sin L dT_0 - K(t - T_0) \sin L dn. \end{aligned} \tag{2.29}$$

ω and e follow from $e\cos\omega$ and $e\sin\omega$. The time of periastron passage T is found from $T_0 + \omega/n$, where T_0 is the corrected time at the instant at which the mean anomaly $M = -\omega$. If the eccentricity is larger than about 0.05, a second iteration is performed using Equation 2.23.

The spectroscopic data of 20 Leonis and α Equulei were used with software developed to perform these least–squares corrections. Two programs were obtained from Scarfe; one is applicable to single–lined binaries while the other is meant to correct simultaneously the orbital elements of eccentric–orbit double–lined binaries. A program by Barlow was used to obtain least–squares corrections to the elements for circular orbits. Detailed descriptions of the programs will not be given here; suffice it to say that the user supplies the preliminary elements and the programs perform the least–squares fits and iterate until the corrections become negligible.

2.2 Eclipsing Binaries

2.2.1 Description

A plot of a star's change in brightness over time is called a light curve. Time is usually expressed as the orbital phase, given by

$$\theta = \frac{2\pi}{P}(t - t_0) \tag{2.30}$$

where P is the period and t_0 is the time of primary minimum. The light data are converted from magnitudes to intensities ℓ by

$$\ell = 10^{-0.4\Delta m} \tag{2.31}$$

where Δm is the difference between the magnitude observed and that at maximum light.

The light curve of an eclipsing binary is a function of a set of unknown elements. Effects which occur when, for example, the two stars are close enough to affect each other's shapes or surface light distributions, result in many unknown elements and therefore a complicated analysis. Only the simplest version, the spherical model, will be discussed here; in most cases it is sufficient to obtain preliminary elements which then may be refined. The spherical model assumes two spherical stars which move in circular orbits with a known period P about a constant centre of mass. Eclipses are symmetrical, of equal duration, and spaced by exactly half a period. The light outside of eclipse is taken to be constant. There are five parameters associated with the spherical model: the radii of the two stars, the fraction of light from each star, the limb–darkening (assumed to be the same for each star) and the orbital inclination. Each of these will be discussed below.

The radii of the two stars in terms of the orbit radius are denoted by r_g and r_s for the larger and smaller star, respectively, and the ratio of these is defined by $k \equiv r_s/r_g$. The total light from the system is given in terms of the fractional intensities of the two stars as $L_g + L_s = 1$. The observed surface brightness of a star decreases toward the limb because of the longer light paths through the stellar atmosphere. This is known as limb–darkening and is denoted by x; it appears in the equation pertaining to the distribution of brightness across the disk of the star:

$$I(\alpha) = I(0)(1 - x + x\cos\gamma) \tag{2.32}$$

where I(0) is the surface brightness at the centre of the observed stellar disk and γ is the angle between the line of sight and the radius vector from the centre of the star. The inclination i is illustratively defined in Figure 2.3.

Two quantities which are closely related are p and δ. p is called the geometrical depth and gives the extent of the eclipse at any phase θ. δ is the apparent separation of the centres of the stellar disks. These two quantities are related by

$$\delta = r_g + pr_s \tag{2.33}$$

$$= r_g(1 + kp). \tag{2.34}$$

Figure 2.3 serves to illustrate another equation for δ, which is known as the geometrical relation and is given by

$$\delta^2 = \cos^2 i + \sin^2 \theta \sin^2 i = 1 - \cos^2 \theta \sin^2 i \tag{2.35}$$

or

$$r_g^2(1 + kp)^2 = \cos^2 i + \sin^2 \theta \sin^2 i. \tag{2.36}$$

This is the fundamental equation used in many solution methods.

Most light curves exhibit two eclipses, a deeper primary and a shallower secondary eclipse. An occultation is an eclipse of the smaller star by the larger, and can be either total or partial. An eclipse of the larger star by the smaller is called a transit, and can be either annular or partial. In the spherical model, the areas eclipsed in occultation and transit are equal, implying that the primary eclipse is due to the eclipse of the star with greater surface brightness. The symmetry also implies that any light curve contains either a total and an annular eclipse, or two partial eclipses.

The type of eclipses may be determined from the shape of the light curve. A total eclipse will give a light curve with a flat minimum, which is very useful since the magnitudes of the two components are directly known; the

Figure 2.3: Illustration of the geometrical relation using great circles.

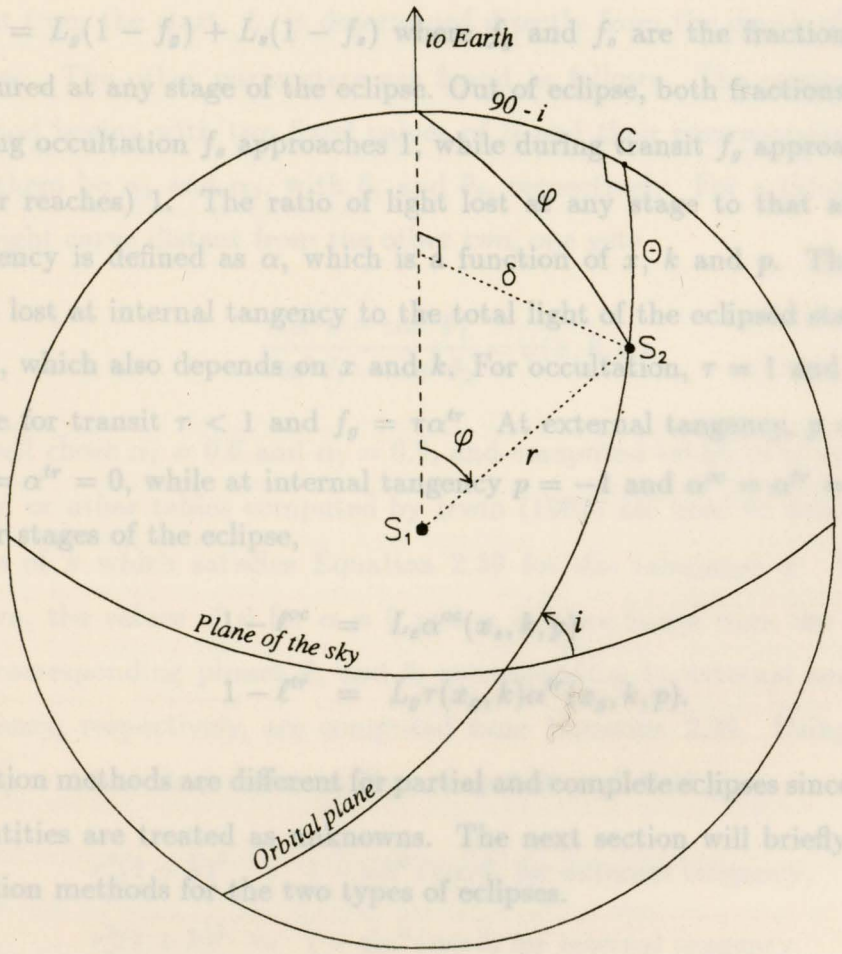

Notes: S_1 and S_2 are the centres of the two stars in the system. C represents conjunction, or the point at which θ (the phase, or longitude from conjunction) is equal to zero. The quantities r, δ and i have been defined in the text.

minimum light level is that of the larger star. An annular eclipse gives a gently rounded minimum due to limb–darkening, while a partial eclipse, the most common type, gives a sharply curved minimum.

There are several photometric relations which pertain to the eclipses. The light received from the system at any phase is denoted by ℓ, and is given by $\ell = L_g(1 - f_g) + L_s(1 - f_s)$ where f_g and f_s are the fractions of light obscured at any stage of the eclipse. Out of eclipse, both fractions are zero; during occultation f_s approaches 1, while during transit f_g approaches (but never reaches) 1. The ratio of light lost at any stage to that at internal tangency is defined as α, which is a function of x, k and p. The ratio of light lost at internal tangency to the total light of the eclipsed star is given by τ, which also depends on x and k. For occultation, $\tau = 1$ and $f_s = \alpha^{oc}$, while for transit $\tau < 1$ and $f_g = \tau\alpha^{tr}$. At external tangency, $p = +1$ and $\alpha^{oc} = \alpha^{tr} = 0$, while at internal tangency $p = -1$ and $\alpha^{oc} = \alpha^{tr} = 1$. At all other stages of the eclipse,

$$1 - \ell^{oc} = L_s\alpha^{oc}(x_s, k, p) \tag{2.37}$$

$$1 - \ell^{tr} = L_g\tau(x_g, k)\alpha^{tr}(x_g, k, p). \tag{2.38}$$

Solution methods are different for partial and complete eclipses since different quantities are treated as unknowns. The next section will briefly describe solution methods for the two types of eclipses.

2.2.2 Solution Methods

If it is assumed that the limb–darkening is known, then the spherical model reduces to the four parameters L_g, r_g, k and i. Several methods have been devised for determining these parameters from the light curve, but the true pioneer in this field is Russell, who in his first paper on the subject (Russell,

1912) described a general solution for light curves. As it is the basis from which the other methods were developed, Russell's procedure will be outlined here.

Complete Eclipses (Russell's Method)

Right from the start, L_g is determined directly from the depth of the total eclipse. The other parameters are found as follows. The original Russell method begins with two fixed values of α and their corresponding phases. Let them be α_1 and α_2, with θ_1 and θ_2, respectively. For a third point on the light curve distant from the other two, one gets

$$\frac{\cos^2\theta - \cos^2\theta_1}{\cos^2\theta_1 - \cos^2\theta_2} = \psi(x, k, \alpha). \tag{2.39}$$

Russell chose $\alpha_1 = 0.6$ and $\alpha_2 = 0.9$, and computed tables of ψ accordingly. They, or other tables computed by Irwin (1962) are used to determine the value of k which satisfies Equation 2.39 for the tabulated ψ. Once k is known, the values of ψ for $\alpha = 0$ and $\alpha = 1$ are found from the table and the corresponding phases θ_e and θ_i corresponding to external and internal tangency, respectively, are computed from Equation 2.39. Using the fact that $p = \pm 1$ at these instants, Equations 2.35 and 2.36 give

$$r_g^2(1+k)^2 = 1 - \sin^2 i \cos\theta_e \text{ for external tangency,} \tag{2.40}$$

$$r_g^2(1+k)^2 = 1 - \sin^2 i \cos\theta_i \text{ for internal tangency.} \tag{2.41}$$

Thus r_g and i can be determined.

Partial Eclipses (The Russell–Merrill Method)

In this case, the light lost at internal tangency is unknown since no internal contacts occur. During each eclipse, the quantity $\ell/\ell_0 = \alpha/\alpha_0 = n$ is

known as a function of phase, where ℓ_0 is the light lost at eclipse minimum. α_0 (the value of α at mid–eclipse) is also unknown, hence it is used as the fourth unknown in addition to k, i and r_g. Both eclipses are required for reasons which will become clear shortly.

The method begins by choosing a base point on the light curve, namely the point $n = 0.5$ (halfway between maximum and minimum light) and noting its corresponding phase $\theta_{n=0.5}$. By dividing this value of θ into the phase at any other point n distant from 0.5 and 1, an equation (known as the shape relation) is obtained:

$$\frac{\sin^2 \theta_n}{\sin^2 \theta_{n=0.5}} = \chi(k, \alpha_0; n, x). \tag{2.42}$$

χ is tabulated as a function of k and α_0 for $n = 0.2$ and 0.8, and an assumed value of x. For any n, the calculated value of χ gives α_0 as a function of k. These are plotted as a curve. This equation gives only one well–determined relation between α_0 and k since the curve based on another point on the same eclipse runs nearly parallel to the first curve. However, the other eclipse gives a relationship between the two quantities which *is* different from the shape relation.

The second relation is called the depth equation and it utilizes the minima of both eclipses. Therefore, even if the other eclipse is small or poorly defined, it still can be used. If the ratio of the fractions of light obscured at any stage is defined as

$$q = \frac{f^{tr}}{f^{oc}}, \tag{2.43}$$

or

$$q = \frac{1 - \ell^{tr}}{\alpha^{oc} + \ell^{oc} - 1} \tag{2.44}$$

then at mid–eclipse $q = q_0$ and Equation 2.44 may be rearranged to give

$$\alpha_0^{oc} = (1 - \ell_0^{oc}) + \frac{1 - \ell_0^{tr}}{q_0}, \text{ with} \tag{2.45}$$

$$k = k(x_g, x_s, \alpha_0^{oc}, q_0). \tag{2.46}$$

Several values of q_0 are chosen and α_0 calculated from Equation 2.45. The corresponding values of k are found from tables of the function in Equation 2.46. Once plotted, this curve will intersect the first one, yielding the true k and α_0. The values for r_g, i and L_g follow.

Note that it is not known beforehand whether primary minimum is an occultation or a transit. Therefore, both cases have to be tried. For example, if it is assumed first that the primary minimum is an occultation, its depth is used as ℓ_0^{oc} and χ is calculated using the tables corresponding to occultation. If transit, then the values for ℓ_0^{oc} and ℓ_0^{tr} are exchanged and χ is computed using the transit tables.

Chapter 3

Photoelectric Photometry

3.1 Introduction

Photoelectric photometry of stars requires a sensitive detector, usually a photomultiplier tube, in order to provide a measurable signal. This type of photometry also involves the use of filters which allow observations to be made in specific wavelength regions. There are several filter systems which may be employed, and each system has its own advantages and disadvantages. An explanation of the different filter systems will not be included in this work, except for the Strömgren filter system; the reader is directed to the texts by Henden and Kaitchuck (1982), and by Hall and Genet (1982), which describe in detail some of the other systems.

As was mentioned previously, 20 Leonis is a triple system consisting of a spectroscopic binary and a δ Scuti visual companion. In addition to spectroscopic observations, photometric observations of 20 Leonis were obtained in order to confirm the variability of the δ Scuti component of the system and to check for multiple periods. These observations were also used to determine whether or not the close pair undergoes eclipses.

The photometry was performed at San Diego State University's Mount Laguna Observatory, located near San Diego, California. A 0.61 m telescope

Table 3.1: Parameters for the 0.61 m telescope at Mt. Laguna Observatory

Parameter	Value
Scale at focal plane	17.3 ″/mm
Focal length	12.0 m
f–ratio	19.7
Dead time of pulse counter	60.0 ns

and single channel photometer, equipped with Strömgren *uvby* filters and a thermoelectrically cooled EMI 6256 photomultiplier tube, were used to obtain the observations. Pertinent information about the telescope system is given in Table 3.1. Other details about the telescope and its operation may be found in the user's manual.

3.2 The Strömgren Photometric System

The Strömgren *uvby* photometric system is known as an intermediate bandwidth system, and consists of the four filters u, v, b and y. The v, b and y filters are all interference filters, and u is a composite glass filter (Strömgren, 1963). The half widths of the filters are on average 200 angstroms (except for u), as compared to 900 angstroms for the the Johnson UBV filters. The central wavelengths and full widths at half transmission of the *uvby* filters, as well as the maximum transmission of the filters are presented in Table 3.2.

The y (yellow) filter is centred in the middle of the visual part of the electromagnetic spectrum, and corresponds closely with the V filter of the Johnson system. This filter transmits no strong spectral features in early

Table 3.2: Filters used in the Strömgren system. Wavelengths and full widths are from Strömgren (1963); maximum transmissions are taken from figures by Crawford (1966).

Filter	Central Wavelength (Å)	Full Width at Half Transmission (Å)	Maximum Transmission (%)
y	5470	230	52
b	4670	180	47
v	4110	190	46
u	3500	300	44

Note: The maximum transmissions for a combination of Schott glass filters chosen by Graham (1982) to reproduce as closely as possible Johnson's original UBV system are 80, 40 and 70 % for the U, B and V bandpasses, respectively.

type stars, and because the filter is not very wide, the red limit is set by the filter itself, and not by the detector, as is the case with the original UBV system. The b, or blue, filter is positioned such that the effects of line blanketing are reduced, especially for stars of early spectral type. The v (violet) filter is located in the region of strong blanketing, yet is still longwards of the Balmer limit at 3647 angstroms. The u, or ultraviolet, filter is located completely to the short wavelength side of the Balmer discontinuity. Thus, a measurement of both the height of the Balmer discontinuity and the amount of line blanketing is possible. Figure 3.1 is a schematic diagram of a stellar spectrum (spectral type mid–F), showing the continuum (solid black line) and the placement of the four filters. It is clear from this diagram that both b and y are nearly free from the effects of line blanketing. Therefore, the quantity $(b - y)$ is a good indicator of the colour and effective temperature of the star. Also, note that if there were no blanketing, the slope of the

Figure 3.1: Theoretical continuum of a stellar spectrum (absorption lines are not shown) and the placement of the four Strömgren filters. From Henden and Kaitchuck (1982), p. 56.

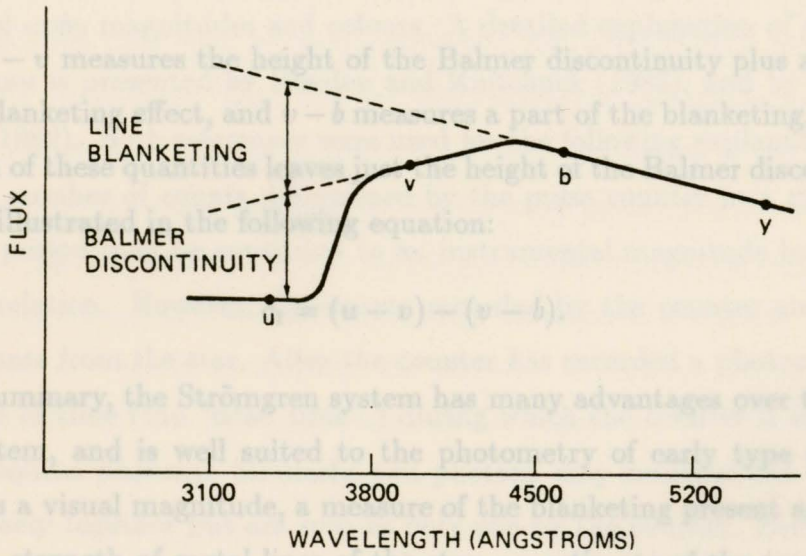

continuum would be nearly constant and $(b-y) \approx (v-b)$. However, the quantity $(v-b)$ is affected by blanketing, so $(v-b)-(b-y)$ is used as an indication of the strength of the blanketing, or in other words, the intensity of the metal lines in the v band. A new quantity m_1, known as the metal index of the star, may then be defined as

$$m_1 = (v-b)-(b-y). \tag{3.1}$$

Since $u-v$ measures the height of the Balmer discontinuity plus a fraction of the blanketing effect, and $v-b$ measures a part of the blanketing, the subtraction of these quantities leaves just the height of the Balmer discontinuity. This is illustrated in the following equation:

$$c_1 = (u-v)-(v-b). \tag{3.2}$$

In summary, the Strömgren system has many advantages over the Johnson system, and is well suited to the photometry of early type stars. It provides a visual magnitude, a measure of the blanketing present and therefore the strength of metal lines of the star, an estimate of the temperature from the quantity $(b-y)$ and a measure of the height of the Balmer discontinuity. Since the system is almost completely filter defined, there is little dependence on the photocell. Effects due to the filters' bandwidths, such as second order colour terms in the extinction corrections or transformation equations are greatly reduced, and can be neglected (especially in differential photometry), so data reduction is simplified. The only major disadvantages of this system are that the narrower filters allow only observations of relatively bright stars, and the peak transmissions of the filters are lower than those of the Johnson UBV system.

3.3 Photometric Reductions

The pulse counter of the telescope records the number of photons arriving at the telescope from the star. These counts may be converted into instrumental magnitudes and colours (magnitudes and colours as determined by the photometric system of the telescope). These magnitudes and colours may then be corrected for effects due to the earth's atmosphere, and converted to standard *uvby* magnitudes and colours. A detailed explanation of reduction techniques is presented by Henden and Kaitchuck (1982), and by Hall and Genet (1982). Both references were used for the following explanation.

The number of counts determined by the pulse counter in a given integration period may be converted to an instrumental magnitude by use of a simple relation. However, the counts recorded by the counter are not the true counts from the star. After the counter has recorded a photon, there is a period of time (the "dead time") during which the counter is insensitive to subsequent photons. Similarly, two photons may arrive at the telescope very closely together but are seen as only one by the counter. Even though the dead time is usually only a few tens to hundreds of nanoseconds, a large error in the number of photons counted may occur, especially for bright stars. Therefore, the number of photons recorded by the counter first must be corrected for dead time, using the equation

$$N = \frac{n}{1 - Dn} \tag{3.3}$$

where n is the observed counts per second, D is the dead time of the counter and N is the counts per second corrected for dead time. This correction should be performed for both star counts and sky counts, especially if the sky is bright due to city lights or a bright moon.

An instrumental, sky–subtracted magnitude m' is given by

$$m' = -2.5 \log [\frac{N_{star}}{N_{sky}}] \tag{3.4}$$

where N_{star} and N_{sky} are the dead–time–corrected counts per second for the star and the sky respectively. The standard deviation in these counts may be taken to be the square root of the counts, if Poisson statistics are obeyed. This deviation may then be easily converted into a magnitude error. Note that these magnitudes have not yet been corrected for effects due to the earth's atmosphere, such as extinction. Briefly, extinction is the dimming of starlight as it passes through the earth's atmosphere, and is determined by observing non-variable stars at different air masses, plotting instrumental magnitudes versus air mass and calculating the slope of the graph. Air mass is just the amount of atmosphere the observer is looking through, and is defined such that the light from stars at the zenith travel through one air mass, and stars between the horizon and zenith have air masses greater than one. The air mass is given to a good approximation by

$$X \approx (\sin \phi \sin \delta + \cos \phi \cos \delta \cos H)^{-1} \tag{3.5}$$

where ϕ is the latitude of the observer, δ is the star's declination and H is the hour angle in degrees. This approximation is valid provided the star is more than about thirty degrees above the horizon. Below this, the curvature of the earth must be taken into account. The out–of–atmosphere magnitude (the magnitude corrected for extinction) is given by the equation

$$m_0 = m' - k'_m X \tag{3.6}$$

where m' is the instrumental magnitude, k'_m is the atmospheric extinction and X is the air mass.

Once the out–of–atmosphere magnitudes have been calculated, they may be transformed to a standard system. The transformation coefficients are determined by observing standard stars, which are stars having known magnitudes and colours. The sample should contain stars having different spectral types and the stars should be observed every night over a wide range of air masses. The equation used to transform between instrumental and standard magnitudes in any filter is given by

$$m_{std} = m_0 + CT(b-y)_{std} + Z \tag{3.7}$$

where m_0 is the extinction– corrected magnitude found from Equation 3.6, CT is the colour term coefficient, $(b-y)_{std}$ is the standard $(b-y)$ colour of the star and Z is the zero point constant of the photometric system. The colour transformation equation is given by

$$C_{std} = SF(C_0) + CT(b-y)_{std} + Z \tag{3.8}$$

where C_0 is the out–of–atmosphere colour, SF is the scale factor between C_0 and C_{std}, and Z is the zero point as before. In both equations, the presence of CT indicates a dependence on $(b-y)$ colour. This is usually regarded as a second order effect, and the colour term coefficient is often set to zero.

The scale factors and colour coefficients describe the differences between the system's filters and the original filters used to obtain standard magnitudes and colours. If the instrumental system exactly matched the original system, the scale factors of the filters would be equal to one, and the colour coefficients would be exactly zero. This is rarely the case, and the deviation determines how far "off" the filters are in wavelength. A value of the scale factor greater than, or less than, one indicates that the central wavelengths of the two filters used to formulate a certain colour (u and b, say) are closer together, or farther apart, than the original filters. Similarly, a negative (or positive)

value of the colour coefficient implies that a filter in the instrumental system lies to the red (or blue) of the standard filter. According to Hall and Genet (1982), any deviation in these coefficients greater then about 0.1 from the ideal value indicates that the instrumental filters are quite different from the standard filters, and the linear equations above should not be used since the transformation is probably nonlinear.

The zero points of the instrument are additive constants which are required in order to obtain a correct apparent magnitude. These constants are determined by several factors, such as the telescope aperture, the sensitivity of the photomultiplier, the filters, the voltage supplied to the photomultiplier and the integration time, to name a few. The zero point should be calculated every night, since there are several things which can occur to change it, such as realuminizing the mirror, dirtying the filters and altering the photomultiplier voltage. Exposing the photocathode to strong light will damage it, resulting in a zero point change. However, it is possible to keep the zero point nearly constant from night to night, and as will be explained in Section 3.4, differential photometry requires only that the zero point remain constant for short periods of time.

These coefficients are obtained by means of the method of linear least squares. First, the raw magnitudes and air masses of the standard stars are plotted to obtain extinction coefficients for each filter. The extinction is then used to calculate instrumental, extinction corrected magnitudes. These magnitudes (or colours) are then plotted against the standard magnitudes (or colours) to obtain transformation coefficients and zero points. The transformation coefficients and zero points should be calculated every night; they should remain fairly constant but as was explained above, any changes to the system will result in a corresponding change in the coefficients and zero points. An explanation of the programs used to compute these coefficients

for 20 Leonis will be included in Chapter 4.

3.4 Differential Photometry

A standard method of photometry involves observing several program stars situated all over the sky, along with standard stars, in order to determine standard magnitudes of the program stars. The extinction and transformation coefficients are also determined for the whole night. This type of photometry is known as all–sky photometry, and is subject to several strict conditions. In order to determine the extinction accurately, the sky must be of consistently good quality for the whole night, and the observing site must be as dark as possible. In contrast, differential photometry involves observing only one program star (usually variable in magnitude) and one (non–variable) comparison star during the night. In this type of photometry, the comparison star is chosen so that it is as close in the sky to the variable as possible. Also, the differences in magnitude between the comparison and variable are determined, which means that many of the critical conditions necessary for all–sky photometry are not really required for differential photometry, since most of the bad effects simply cancel. In differential photometry, it is possible to obtain accuracies of at least $\pm$ 0.007 in differential magnitudes.

The equations describing atmospheric extinction and the transformation to a standard system are obtained by simply subtracting the equations for the comparison star from the equations for the variable star. The differences in the quantities involved are represented by the symbol Δ. The first equation below is used to calculate the differential instrumental magnitude, the second and third are then used to calculate the standard differential magnitudes and

colours, ΔM_{std} and ΔC_{std} respectively.

$$\Delta m_0 = \Delta m' - k'\Delta X \tag{3.9}$$

$$\Delta M_{std} = \Delta m_0 + CT(\Delta(b-y)_{std}) \tag{3.10}$$

$$\Delta C_{std} = SF(\Delta C_0) \tag{3.11}$$

In the above equations, SF and CT are as previously defined, and ΔX is the differential air mass, which is a very small quantity if the two stars are close together in the sky. Note that in differential photometry, the zero points cancel (provided the zero point of the instrumental system remains constant during an integration). This makes the equations even simpler to use.

This method of photometry has many advantages. Observations may be made on nights when the sky is of variable transparency, and when only sections of the sky are clear. If the variable and comparison stars are sufficiently close together in the sky, the sky transparency is usually the same in that small region containing the two stars. As an example, if a patch of cirrus cloud is contaminating the light from one star, it will also contaminate the other star's light by approximately the same amount. In the subtraction, then, this effect cancels. Another benefit of close proximity is that only a small correction is needed for differential atmospheric extinction. This is apparent from Equation 3.9. If the two stars are close in magnitude and spectral type, then only a small correction is needed for the differential transformation to a standard system, which is evident from Equation 3.10. Finally, if the comparison and variable are observed within a few minutes of each other (assuming simultaneous photometry is not being performed), then the system's zero point need only hold constant for that length of time. Even if it does drift gradually, it would still be manageable since the comparison star is usually observed immediately before and after the variable star, and the average brightness is used in the subtraction. As a consequence, the

differential method was used for the observations to be described in the next chapter.

Chapter 4

20 Leonis

4.1 Introduction

As was discussed in Chapter 1, 20 Leonis (HR 3889, HD 85040) is a member of a class of systems known as spectroscopic–visual triples. The photometry, spectroscopy and results of the analysis will be discussed in this chapter. The next two sections will be devoted to the photometric observations and analysis, while the fourth and fifth sections will cover the spectroscopic aspects of the data. A discussion of the results will constitute the sixth section.

4.2 Reduction of the Photometry

20 Leonis was observed at San Diego State University's Mt. Laguna Observatory during the period from February 7 to February 16 (PST), 1989. (Note that it is not possible to observe the three stars separately.) Since the observations were to be used to search for eclipses, it was necessary to predict the times of the eclipses for the observing dates in mind. Using FB's (1977) value for T_0, the heliocentric Julian dates (HJD) at both conjunctions (assumed to be at spectroscopic phases of 0.25 and 0.75) were calculated and the appropriate number of cycles was added to these dates in order to obtain

the dates of the conjunctions during the above period of time. It was predicted that eclipses would occur in the early morning of the odd dates, with primary and secondary eclipses alternating (since the period of the binary is just over 4 days).

Skies were cooperative only for the nights of February 10–12 and 14–16, but the phase coverage was sufficient for modelling any eclipses which might have occurred. The comparison and check stars HD 84497 and HD 86516 were observed as well. Table 4.1 lists the three stars' coordinates for an equinox and equator of 1950.0.

Table 4.1: Coordinates of the program and comparison stars

HD	RA (h m s)	DEC (° ′ ″)
85040	09 47 02.4	+21 24 47.9
84497	09 43 25.0	+20 40 30.0
86516	09 56 41.3	+21 03 39.6

Standard stars were observed every night to obtain transformation coefficients and check for second–order colour terms in the extinction. The properties of these stars may be found in Table 4.3. Three groups of standards were chosen and observed in the following manner. Since the stars ranged in right ascension, a group was observed near the meridian at the beginning of the night, at midnight and before dawn. In addition, the bluest and reddest stars from each group were observed when they were near the horizon; these observations were to be used to look for the second–order extinction terms. Unfortunately, since some of the nights were partly cloudy, it was not always possible to observe the standard stars in the above fashion. However, it was

thought that second–order terms would have a negligible effect on the final results since we were concerned with differential, not absolute, photometry.

The observations of 20 Leonis and the comparison and check stars were performed in the following sequence: program, comparison, check, program, comparison, check, and so on. The sky was observed every two or three cycles of the above sequence. The integration times for the stars and sky were 15 to 20 seconds (depending on the quality of the night) and 10 seconds, respectively. The standard stars were observed for 10 seconds as well, since they were bright and a good signal–to–noise ratio could be obtained within that length of time.

The extinction in each filter was calculated from both the comparison and check stars, for each night of data. The two values agreed within error, and a weighted average was adopted as the nightly extinction. It is clear from Table 4.4 that the values vary widely from night to night. Because of this, calculations requiring extinction coefficients were performed using the nightly values.

Table 4.5 contains the transformation coefficients which were calculated from the standard star observations. The scale factor and zero point were determined for each night, assigned a weight (based on the associated error from the least squares fit), and averaged. It was thought that this procedure would not jeopardize the accuracy of the final results, since the coefficients were quite consistent from night to night.

The coefficients were used to calculate transformed magnitudes and colours for the standard stars, and the residuals were plotted against air mass, universal time and standard $(b - y)$ colour. Any correlations between these quantities could mean that the sky or instrumentation was changing. Since there were no obvious correlations in these data, second–order corrections were not included. The transformation and extinction coefficients were then

used to calculate standard magnitudes and colours for the variable, comparison and check stars.

These data were then run through a program which computed a differential magnitude for each variable star observation, in the following manner. Since each variable measurement was bracketed by two comparison stars, the magnitude of the comparison corresponding to the time at which the variable star was observed could be calculated via linear interpolation between the two comparisons. The differential magnitude was found by subtracting this "fake star" from the variable star. The heliocentric Julian date and sidereal time for each observation were calculated as well. The program also generated a main file containing:

- magnitudes and colours, and their errors, for the program star observations,
- the means and standard deviations of V, $(b-y)$, m_1 and c_1 for the comparison and check stars, and
- differential extinction and transformation coefficients,

as well as files containing the comparison and check star observations, differential magnitudes for the variable star, and differential magnitudes in the sense *check – comparison.*

The program was run twice for each night of data. The first run calculated differential magnitudes in the sense *variable – comparison*, while the second run replaced the comparison by the check star. It was found that both sets of magnitudes gave similar errors, so the the differential *variable – comparison* magnitudes were used in subsequent calculations. Differential *check – comparison* magnitudes were examined to confirm the suitability of these stars as comparisons and to determine the quality of the data. Table 4.2 summarizes the mean magnitudes and standard deviations of the *check –*

comparison data. Except for the first night, the values are consistent, and the standard deviations show that the data are of reasonable quality.

Table 4.2: Mean magnitudes of the differential check data, for each night of observations.

JD 2440000+	No. of Observations	Δm	
		y	b
7568	15	-0.644 ± 0.008	-0.822 ± 0.010
7569	26	-0.633 ± 0.011	-0.815 ± 0.010
7570	15	-0.636 ± 0.007	-0.811 ± 0.009
7572	40	-0.634 ± 0.012	-0.815 ± 0.009
7573	21	-0.636 ± 0.012	-0.816 ± 0.012
7574	28	-0.634 ± 0.009	-0.812 ± 0.010
		v	u
7568	15	-0.930 ± 0.010	-0.598 ± 0.010
7569	26	-0.923 ± 0.009	-0.590 ± 0.014
7570	15	-0.918 ± 0.010	-0.590 ± 0.011
7572	40	-0.925 ± 0.008	-0.594 ± 0.011
7573	21	-0.925 ± 0.010	-0.590 ± 0.011
7574	28	-0.921 ± 0.011	-0.587 ± 0.010

Notes: The means and standard deviations of the complete set of data for each of the filters y, b, v and u are -0.635 ± 0.011, -0.815 ± 0.010, -0.923 ± 0.010 and -0.591 ± 0.012, respectively.

Table 4.3: Standard stars. Coordinates are for an equinox and equator of 2000.0, V, $b-y$, m_1 and c_1 are in magnitudes. From Crawford and Barnes (1970).

HR	RA (h m s)	DEC (° ′ ″)	Sp T	V	$(b-y)$	m_1	c_1
1140	03 44 48	+24 17 22	*B7 IV*	5.45	−0.001	0.105	0.647
1144	03 45 10	+24 50 21	*B8 V*	5.64	−0.022	0.109	0.637
1201	03 53 10	+17 19 38	*F4 V*	5.97	+0.221	0.166	0.610
1269	04 07 00	+29 00 05	*F1 V*	5.23	+0.226	0.159	0.588
1329	04 17 16	+20 34 43	*A3m*	4.94	+0.146	0.235	0.745
1331	04 18 23	+21 34 46	*A8 V*	5.65	+0.175	0.185	0.787
1341	04 19 37	+21 46 25	*A0p*	5.38	−0.094	0.197	0.536
1656	05 07 27	+18 38 42	*G4 V*	5.00	+0.415	0.197	0.332
1662	05 07 38	+18 38 42	*G1 IV*	6.17	+0.398	0.185	0.350
2220	06 14 51	+19 09 23	*F6 V*	5.20	+0.293	0.163	0.448
2241	06 16 27	+12 26 20	*F5 IV*	5.04	+0.284	0.153	0.438
3657	09 13 37	+21 17 00	*A2 V*	6.48	+0.017	0.164	1.094
3815	09 35 40	+35 48 36	*G8 III*	5.41	+0.473	0.304	0.372
3906	09 52 12	+02 27 15	*A0 Vs*	6.03	−0.015	0.136	1.040
3951	10 01 01	+31 55 25	*G2 Va*	5.35	+0.416	0.234	0.388
4753	12 29 27	+24 06 32	*F5 III*	5.48	+0.289	0.172	0.611
4883	12 51 42	+27 32 26	*G0 III*	4.94	+0.435	0.193	0.411
5011	13 16 46	+09 25 27	*F8 V*	5.22	+0.376	0.191	0.383
5017	13 17 32	+40 34 21	*F3 III*	4.73	+0.180	0.231	0.193
5072	13 28 26	+13 46 43	*G2.5 Va*	4.97	+0.446	0.232	0.350
5304	14 10 24	+25 05 30	*F8 IV*	4.83	+0.348	0.175	0.441
5522	14 48 54	−00 50 51	*B9*	6.16	−0.007	0.132	0.996
5633	15 07 20	+18 26 30	*A3 V*	6.02	+0.032	0.190	1.017
5634	15 07 18	+24 52 09	*F5 V*	4.93	+0.287	0.161	0.448

Table 4.4: Extinction coefficients

JD	k'_y	k'_b	k'_v	k'_u
2447568	0.115 ± 0.014	0.155 ± 0.012	0.281 ± 0.015	0.536 ± 0.015
2447569	0.153 ± 0.012	0.198 ± 0.011	0.312 ± 0.012	0.569 ± 0.012
2447570	0.208 ± 0.014	0.282 ± 0.017	0.407 ± 0.019	0.651 ± 0.019
2447572	0.218 ± 0.008	0.278 ± 0.008	0.402 ± 0.008	0.678 ± 0.009
2447573	0.172 ± 0.007	0.232 ± 0.006	0.360 ± 0.006	0.620 ± 0.008
2447574	0.148 ± 0.004	0.197 ± 0.003	0.315 ± 0.005	0.573 ± 0.006

Table 4.5: Transformation coefficients

Quantity	Zero Point	Scale Factor
V	−1.134 ± 0.004	0.047 ± 0.013
$b-y$	1.092 ± 0.003	1.037 ± 0.004
m_1	−0.853 ± 0.035	0.864 ± 0.029
c_1	0.636 ± 0.002	0.983 ± 0.007

4.3 Photometric Analysis

In order to classify the spectrum, the means of $(b-y)$, m_1 and c_1 for 20 Leo were calculated for each night. The means for three of the six nights, however, differed greatly from those found for the other nights. Since the comparison star changed in the same manner, it was concluded that the difference was probably due to poor skies. This conclusion was established further once the observing notes were reviewed. Thus, means of the above quantities were calculated using only the three good nights of data (*ie.*, the nights with lowest extinction), as 0.145 ± 0.005, 0.217 ± 0.008 and 0.914 ± 0.009. A discussion of the spectral type and luminosity class based on these values will follow.

The differential magnitude data were plotted against time to display the δ Scuti variation. Each night's set of data showed the variation to be present, but inconsistent in that the amplitude and phase changed from night to night. Elliott (1974) had found a period of 0.0818 days. A period– finding program was used with the new data to find a period of 0.0826 days. It should be noted that the data containing only the δ Scuti variation were used in the above derivation. Table 4.6 contains the amplitudes (in mags), phase shifts and mean light levels (in mags) in the four bandpasses; Figure 4.1 contains the plots of the data phased on $P = 0.0826$ days. Note the good night–to–night correlation between the parameters. The errors in the amplitude ranged from 0.002 to 0.01, while the errors in the phase shift were usually quite large; typically 0.05 to 0.1. The errors in the mean light level were considerably lower, in the range 0.002 to 0.008. The author realizes that in some of these plots (especially in the u bandpass), any δ Scuti variation is almost completely obscured by the scatter in the data. This scatter is due to a number of factors such as observing error, poor sky conditions and the

inherent noisiness of δ Scuti light curves.

Table 4.6: Parameters of the δ Scuti light curves

JD	A	Shift	$\overline{\Delta m}$	JD	A	Shift	$\overline{\Delta m}$
	y				b		
2447568	0.015	0.24	−1.292	2447568	0.018	0.25	−1.436
2447569	0.016	0.36	−1.299	2447569	0.020	0.35	−1.450
2447570	0.015	0.46	−1.288	2447570	0.018	0.43	−1.431
2447572	0.008	0.37	−1.288	2447572	0.008	0.32	−1.436
2447573	0.010	0.42	−1.299	2447573	0.010	0.46	−1.450
2447574	0.007	0.35	−1.283	2447574	0.008	0.34	−1.432
	v				u		
2447568	0.020	0.25	−1.516	2447568	0.018	0.21	−1.127
2447569	0.023	0.35	−1.534	2447569	0.021	0.34	−1.137
2447570	0.015	0.41	−1.510	2447570	0.015	0.35	−1.120
2447572	0.008	0.31	−1.517	2447572	0.005	0.31	−1.128
2447573	0.007	0.53	−1.531	2447573	0.005	0.46	−1.135
2447574	0.010	0.40	−1.514	2447574	0.006	0.45	−1.124

Figure 4.1: The δ Scuti light curves. Differential magnitudes are plotted against phase. a. JD 2447568

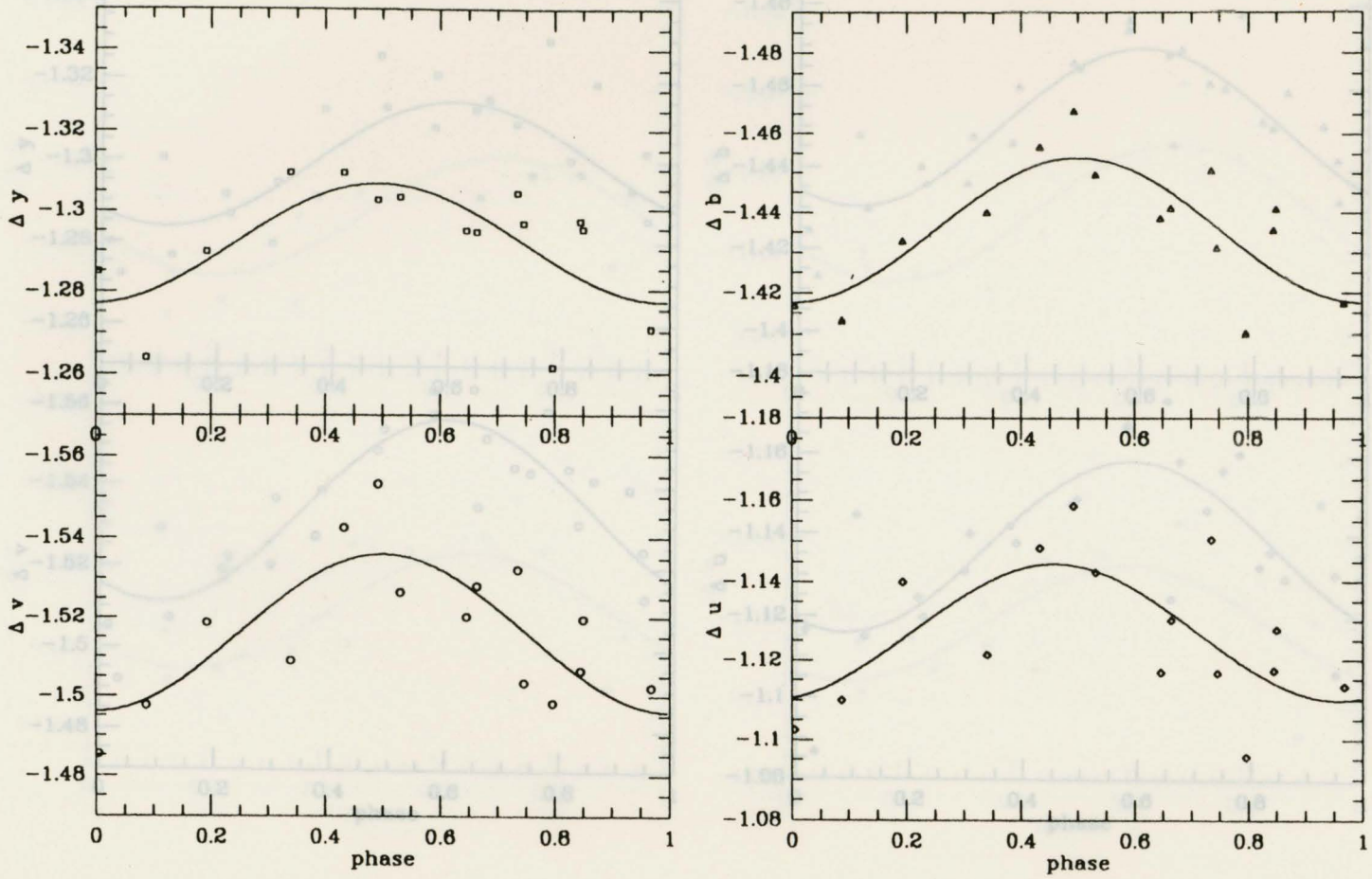

Figure 4.1. b. JD 2447569

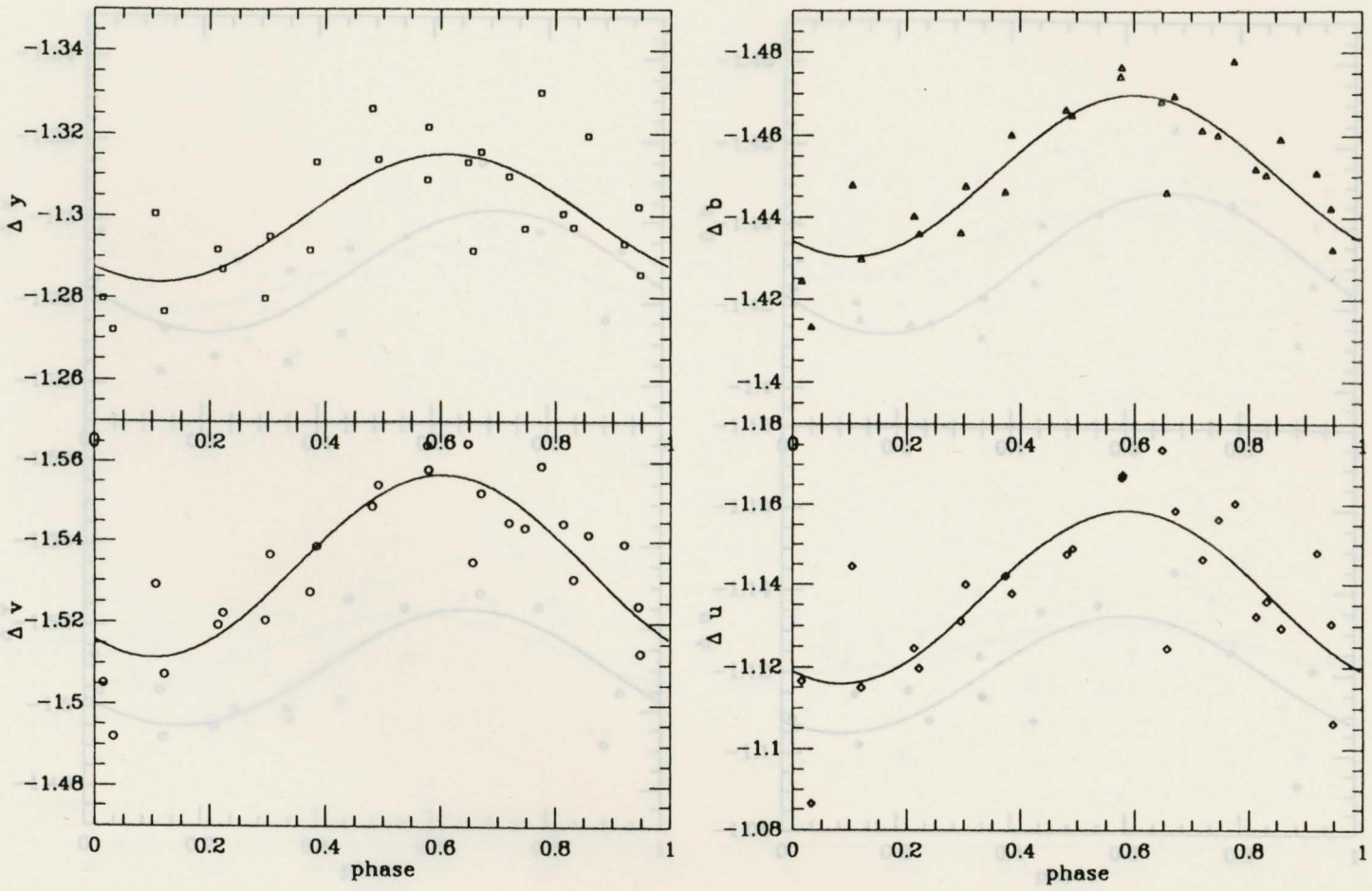

Figure 4.1. c. JD 2447570

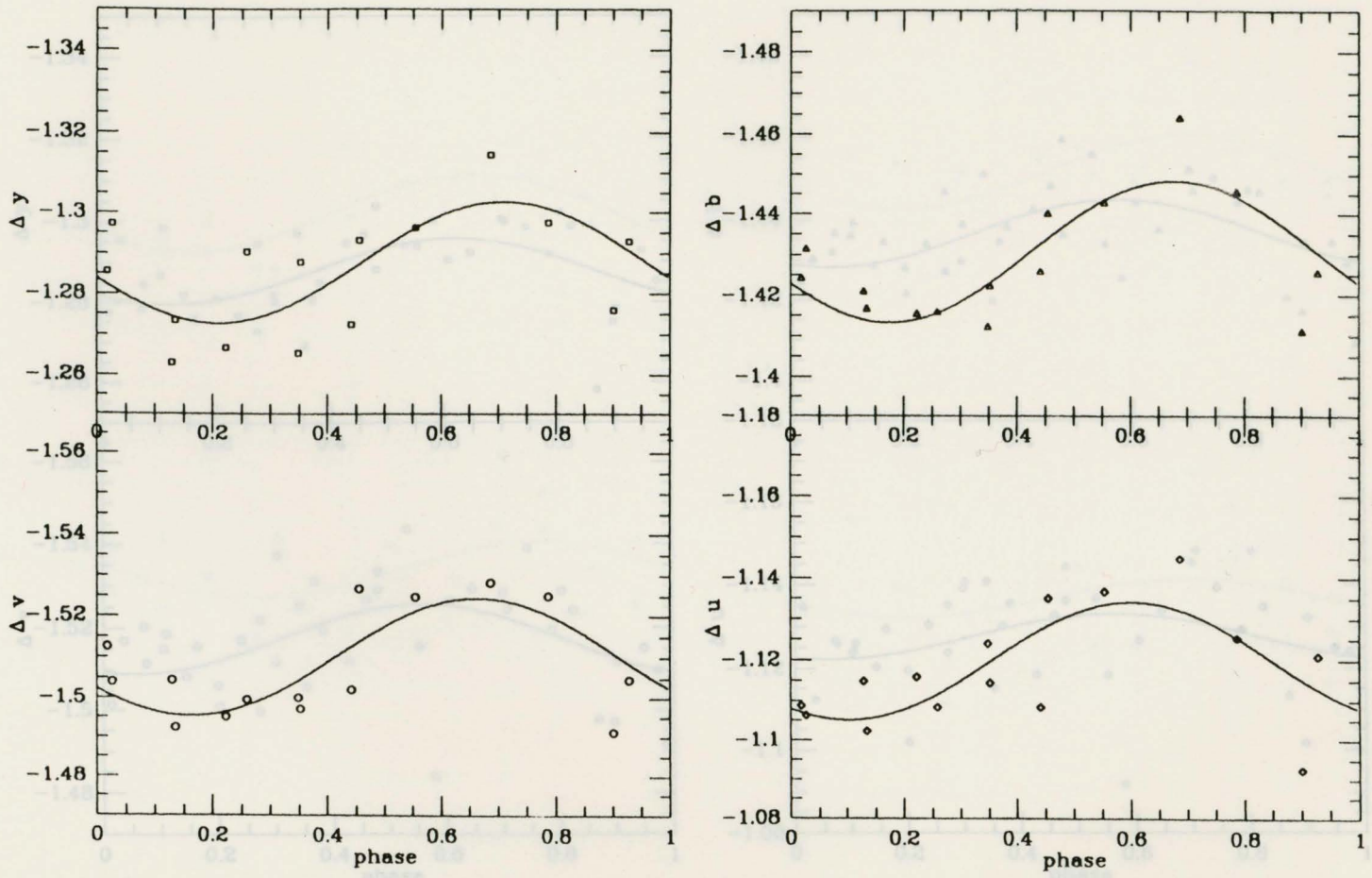

Figure 4.1. d. JD 2447572

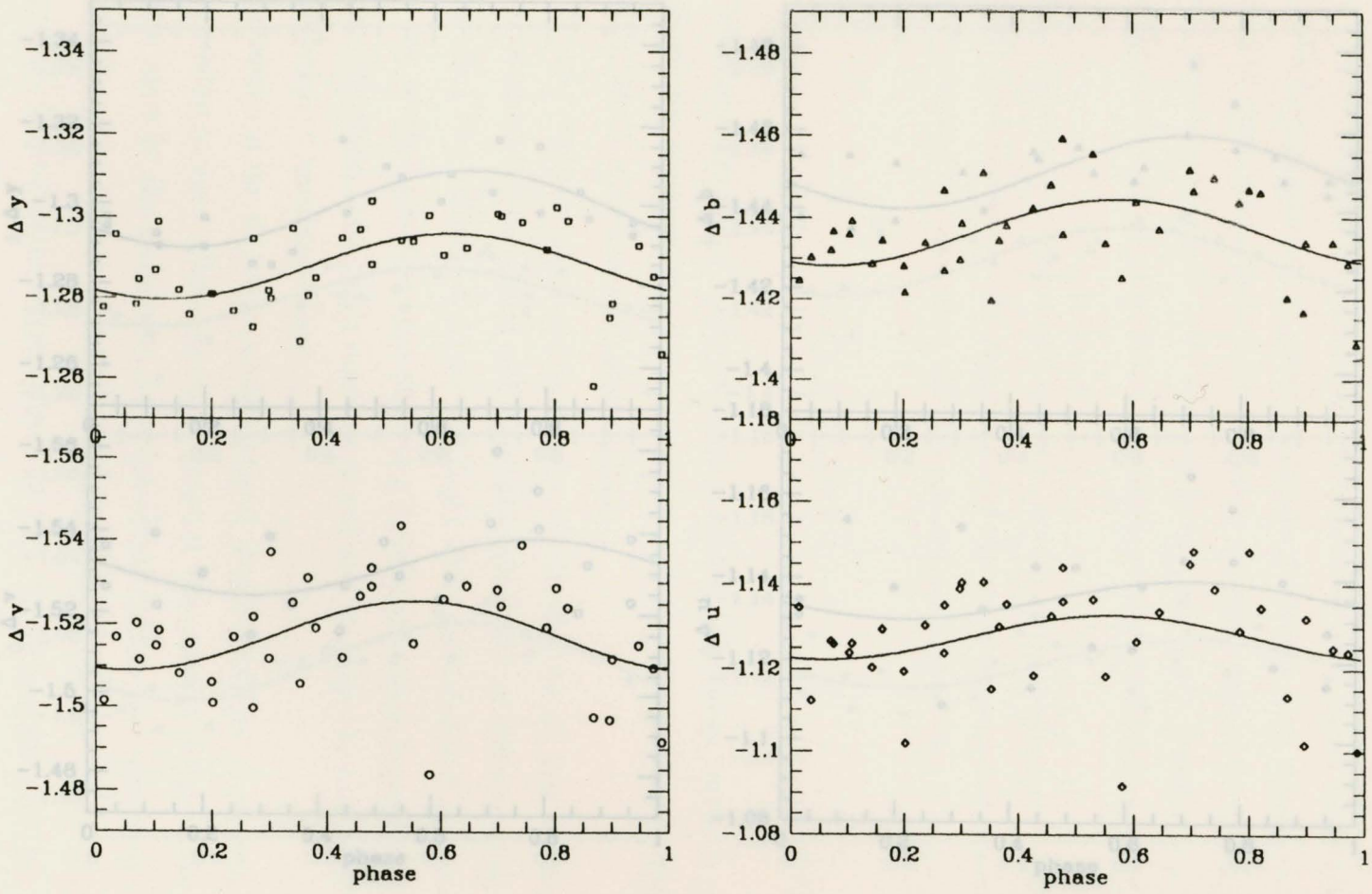

Figure 4.1. e. JD 2447573

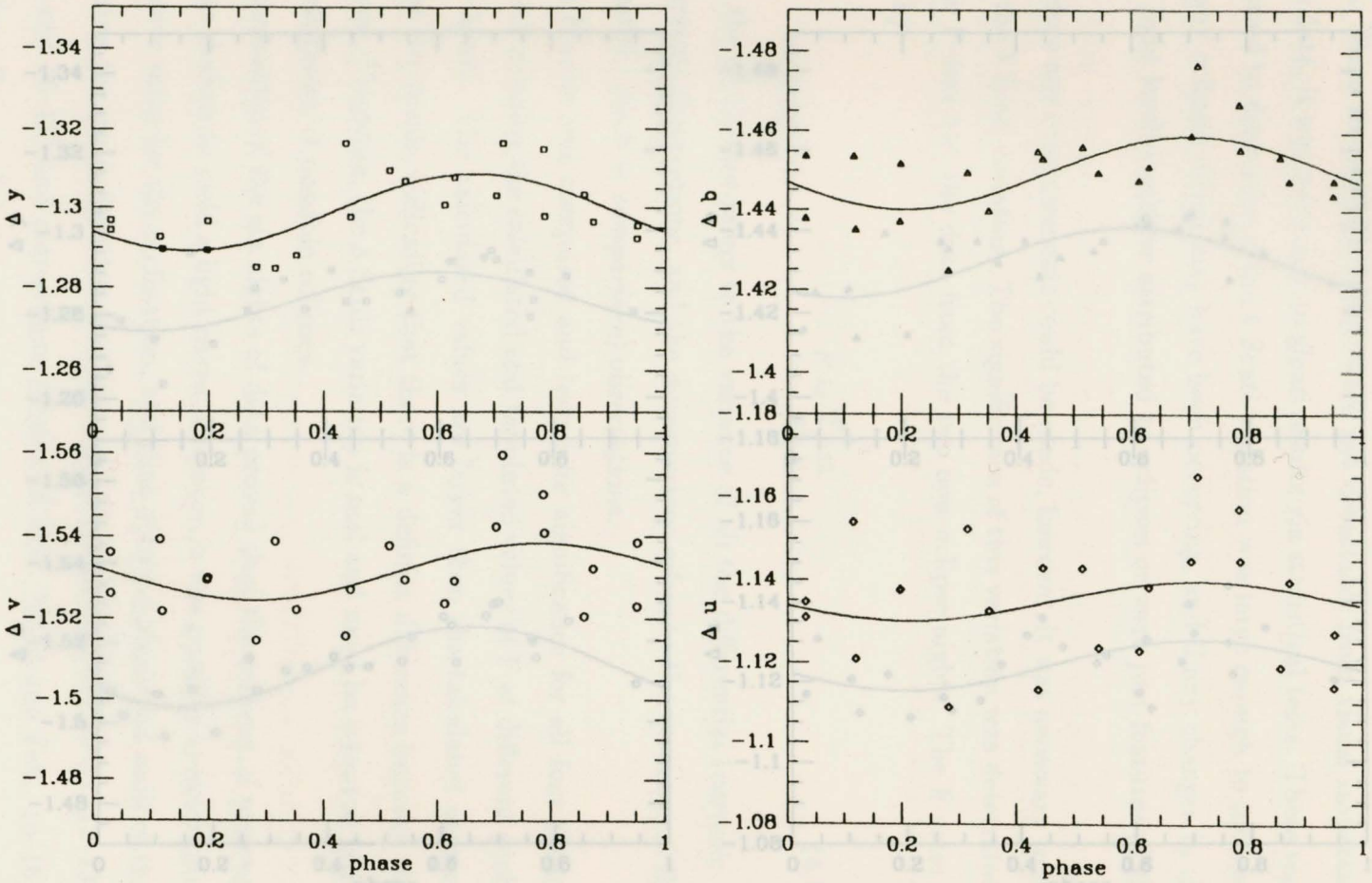

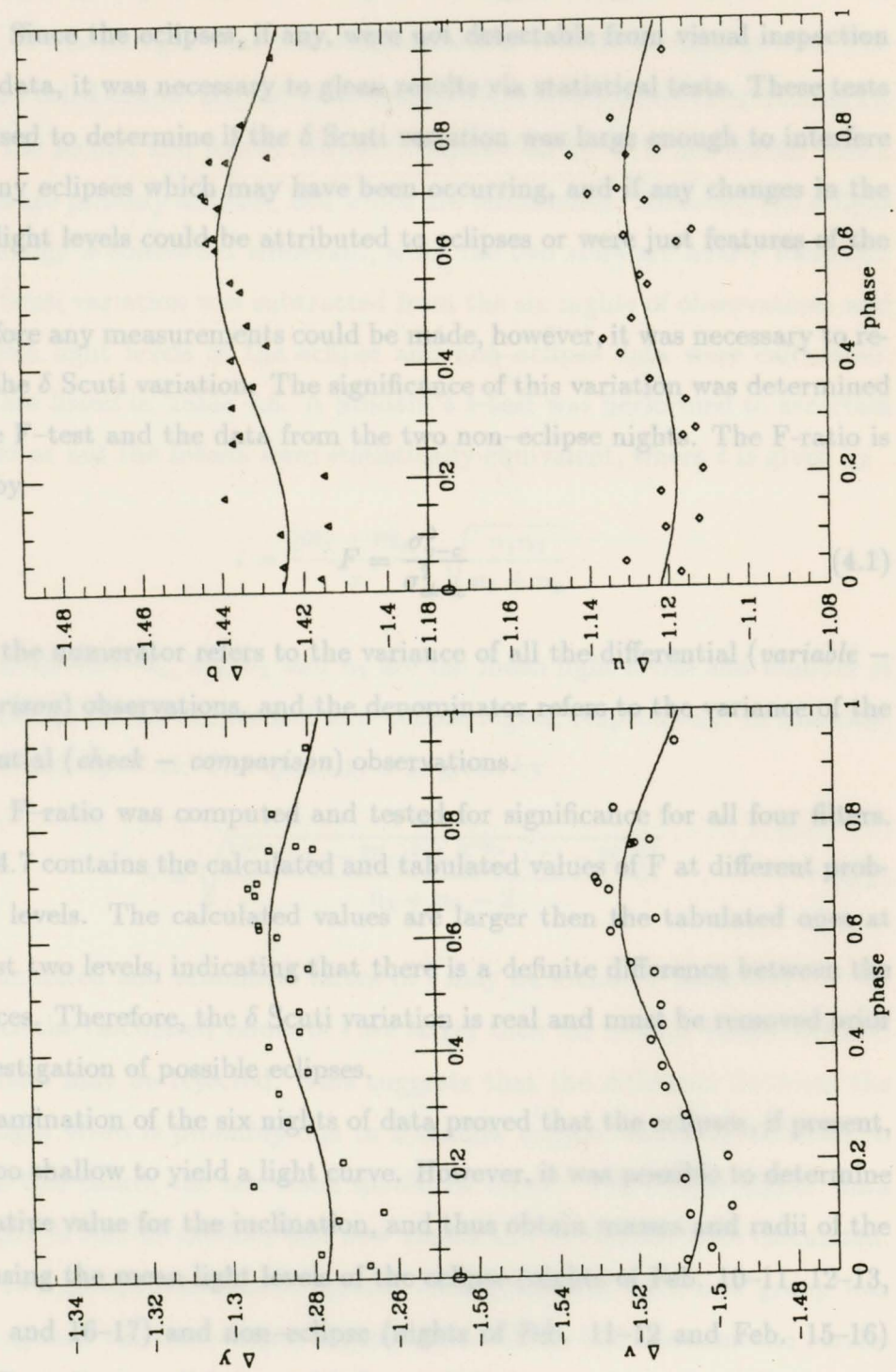

Figure 4.1. f. JD 2447574

The possibility that the close pair undergoes eclipses was also investigated. Since the eclipses, if any, were not detectable from visual inspection of the data, it was necessary to glean results via statistical tests. These tests were used to determine if the δ Scuti variation was large enough to interfere with any eclipses which may have been occurring, and if any changes in the mean light levels could be attributed to eclipses or were just features of the data.

Before any measurements could be made, however, it was necessary to remove the δ Scuti variation. The significance of this variation was determined via the F–test and the data from the two non–eclipse nights. The F-ratio is given by

$$F = \frac{\sigma^2_{v-c}}{\sigma^2_{ck-c}} \tag{4.1}$$

where the numerator refers to the variance of all the differential (*variable* − *comparison*) observations, and the denominator refers to the variance of the differential (*check* − *comparison*) observations.

An F–ratio was computed and tested for significance for all four filters. Table 4.7 contains the calculated and tabulated values of F at different probability levels. The calculated values are larger then the tabulated ones at the first two levels, indicating that there is a definite difference between the variances. Therefore, the δ Scuti variation is real and must be removed prior to investigation of possible eclipses.

Examination of the six nights of data proved that the eclipses, if present, were too shallow to yield a light curve. However, it was possible to determine a tentative value for the inclination, and thus obtain masses and radii of the stars using the mean light levels of the eclipse (nights of Feb. 10–11, 12–13, 14–15, and 16–17) and non–eclipse (nights of Feb. 11–12 and Feb. 15–16) data. Since Barnes, Fekel and Moffett (1977) had assumed that the eclipses

lasted for approximately one–tenth of a full cycle (which translates to 9.6 hours), it was thought that this simple procedure would be appropriate. The first and third eclipse are the same (arbitrarily chosen to be Conjunction 1), as are the second and fourth eclipse (Conjunction 2). It is not known which eclipses are primary eclipses, and which are secondaries. However, the eclipse terminology is somewhat irrelevant, since the two stars are nearly identical. The δ Scuti variation was subtracted from the six nights of observations and the mean light levels of the eclipse and non–eclipse data were calculated. These are listed in Table 4.8. A Student's t–test was performed to ascertain whether or not the means were statistically equivalent, where t is given by

$$t = \frac{|\overline{m}_1 - \overline{m}_2|}{\sigma} \cdot \sqrt{\frac{n_1 n_2}{n_1 + n_2}}. \tag{4.2}$$

The parameters $\overline{m}_1$, $\overline{m}_2$, n_1 and n_2 are the mean light levels and number of observations for the eclipse and non–eclipse nights, respectively. In this case, $n_1 = 96$ and $n_2 = 49$. The quantity σ is given by

$$\sigma = \sqrt{\frac{\sum_{i=1}^{n_1}(x_i - \overline{m}_1)^2 + \sum_{j=1}^{n_2}(x_j - \overline{m}_2)^2}{n_1 + n_2 - 2}}. \tag{4.3}$$

The calculated and tabulated values of t may be found in Table 4.9.

Since the calculated values of t are larger than the critical values, the null hypothesis may be rejected. This suggests that the difference between the mean light levels is probably due to a shallow eclipse. However, in order to confirm this result, the test itself should be tested. The eclipse nights' data were split in half at random and new means and deviations were calculated. These two groups were tested against each other, and each new group was tested against the non–eclipse nights' data. Table 4.10 contains the results of these tests.

Table 4.7: Results of the F–test. Tabulated values are for 49 and 49 degrees of freedom.

Filter	F_{calc}	F_{tab}		
		p = 0.1	p = 0.05	p = 0.01
y	1.27	1.46	1.60	1.95
b	1.79	1.46	1.60	1.95
v	2.59	1.46	1.60	1.95
u	2.10	1.46	1.60	1.95

Table 4.8: Mean light levels for eclipse (E) and non–eclipse (NE) nights. The standard deviations are 0.009 for all values.

Filter	Mean	
	E	NE
y	−1.287	−1.299
b	−1.434	−1.450
v	−1.515	−1.533
u	−1.125	−1.136

Table 4.9: Results of the *t*–test. Tabulated values are for 2 and 143 degrees of freedom.

Filter	t_{calc}	t_{tab}	
		p = 0.05	p = 0.01
y	+ 7.6	+ 1.9	+ 2.7
b	+ 9.9	+ 1.9	+ 2.7
v	+10.5	+ 1.9	+ 2.7
u	+ 5.2	+ 1.9	+ 2.7

Table 4.10: Results of the t–test performed on new data groups. Tabulated values are for 2 and 94 degrees of freedom for the first set, and 2 and 95 for the second and third set.

Data Sets	t_{calc}	t_{tab} p = 0.05	p = 0.01
Groups 1 + 2			
y	+2.1	+2.0	+2.6
b	+0.5	+2.0	+2.6
v	+1.2	+2.0	+2.6
u	+0.3	+2.0	+2.6
Group 1 + No ecl.			
y	+5.3	+2.0	+2.6
b	+8.5	+2.0	+2.6
v	+8.8	+2.0	+2.6
u	+4.1	+2.0	+2.6
Group 2 + No ecl.			
y	+7.7	+2.0	+2.6
b	+9.0	+2.0	+2.6
v	+9.1	+2.0	+2.6
u	+4.6	+2.0	+2.6

It is evident from the table that there is no statistical difference among the eclipse data, and that the difference between the eclipse and non-eclipse data is significant.

One final test may be performed to verify the statement that one cannot distinguish between the primary and secondary eclipses from these data. The *t*–test was used on the Conjunction 1 and Conjunction 2 data; results of this comprise Table 4.11. Since there is no statistical difference between the two distributions, it is safe to conclude that the two eclipses are probably identical. Section 4.6 contains a discussion of these results and a derivation of the inclination and stellar parameters.

Table 4.11: Results of the *t*–test performed on the eclipse data. Tabulated values are for 2 and 94 degrees of freedom.

Filter	t_{calc}	t_{tab}	
		p = 0.05	p = 0.01
y	+1.6	+2.0	+2.6
b	+1.8	+2.0	+2.6
v	+1.5	+2.0	+2.6
u	+1.5	+2.0	+2.6

4.4 The Spectroscopic Observations

FB had obtained 39 triple–lined coudé spectrograms in order to calculate a radial velocity curve for the close pair, and to determine which of the three stars was the δ Scuti. Their data were very convincing for the δ Scuti case; a series of eight spectrograms taken in rapid succession showed that the distant companion was indeed the δ Scuti variable. Their radial velocity curve covered only the maxima and minima; it was hoped that we could obtain velocities which would cover more of the curve. Scarfe obtained radial velocities at eleven dates, on ten of which all three spectra were resolved.

The radial velocities were determined using the Dominion Astrophysical Observatory's (hereafter referred to as DAO) radial velocity scanner (RVS). An excellent discussion of the RVS may be found in Fletcher, et al. (1982); a brief overview will be given here. Please refer to Figure 4.2 for the configuration of the spectrograph and the scanner. It should be noted, however, that this picture is outdated; the Fabry lens was replaced in 1985 by a set of mirrors designed to permit use of a photomultiplier tube with a small cathode. The RVS is located near the focus of the coudé spectrograph of the 1.2 meter telescope at the DAO, and consists of a spectrum mask driven by a stepping motor, a field lens and a photomultiplier tube. The light arrives in focus at the mask via a 45° flat mirror placed at the normal plate holder focus. The transmitted light travels through the mirror network (in place of the Fabry lens in Figure 4.2) to the photomultiplier which counts the photons and records the intensity of the transmitted light.

The mask consists of transparent spectral lines on an opaque background. As it travels across the stellar spectrum (parallel to the dispersion), the intensity of the transmitted light at each step is binned. When the scan is completed, the oscilloscope displays the accumulated counts in each bin,

which form a dip whose minimum corresponds to the point at which the spectral lines matched those of the mask. The computer program fits a parabola to a portion of the dip selected by the observer, and calculates the velocities.

The shape of the dip and therefore the accuracy of the velocity determined is affected by stellar rotation. Since the dip is a convolution of the instrumental profile and the stellar profile, a rotationally broadened stellar profile will cause the dip to appear broad and shallow, thus increasing the error on the derived velocity. The spectral lines of 20 Leonis were rotationally broadened, resulting in uncertainties of 0.6 to 4.6 km/s.

4.5 The Spectroscopic Analysis

Our and FB's data were combined in order to recalculate the orbital elements of the spectroscopic binary. The quality of the velocities was determined by calculating the elements for each component. It was found that star *Aa*'s velocities were of poorer quality than those of *Ab*. The standard error of an observation of unit weight, given by

$$\sigma = \sqrt{\frac{\Sigma(O-C)^2}{N-3}} \tag{4.4}$$

was used to weight the observations in preparation for a simultaneous solution. The standard errors for *Aa* and *Ab* were 3.9 km/s and 2.4 km/s, corresponding to weights of 0.4 and 1.0, respectively. Once properly weighted, orbital elements for the double–lined case were computed. The eccentricity was found to be negligible, and the elements were recalculated assuming $e = 0.0$. Table 4.13 lists the radial velocities, as well as phases and residuals computed from the second set of orbital elements in Table 4.12. The velocities of the visual companion (designated *B*) may be found in Table 4.14.

Figure 4.2: A schematic diagram of the 1.2 m telescope's coudé spectrograph and radial velocity scanner. From Fletcher, et al. (1982).

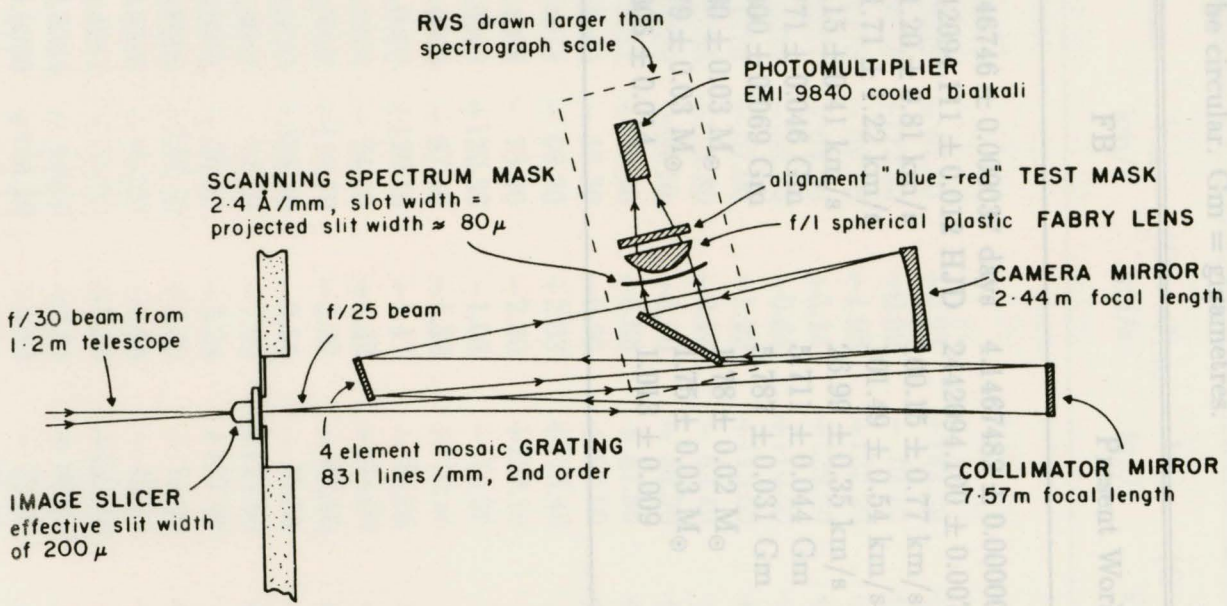

Table 4.12: Orbital elements of 20 Leonis. The first set pertain to FB's data only; the second set are based on the combination of our and FB's data. The orbit is assumed to be circular. Gm = gigametres.

Parameter	FB	Present Work
P	4.146746 ± 0.000037 days	4.1467482 ± 0.0000091 days
T_0	2442094.111 ± 0.012 HJD	2442094.100 ± 0.007 HJD
K_{Aa}	101.20 ± 0.81 km/s	100.15 ± 0.77 km/s
K_{Ab}	101.71 ± 1.22 km/s	101.49 ± 0.54 km/s
γ	27.15 ± 0.41 km/s	26.99 ± 0.35 km/s
$a_{Aa} \sin i$	5.771 ± 0.046 Gm	5.711 ± 0.044 Gm
$a_{Ab} \sin i$	5.800 ± 0.069 Gm	5.787 ± 0.031 Gm
$M_{Aa} \sin^3 i$	1.80 ± 0.03 $M_\odot$	1.78 ± 0.02 $M_\odot$
$M_{Ab} \sin^3 i$	1.79 ± 0.03 $M_\odot$	1.75 ± 0.03 $M_\odot$
M_{Aa}/M_{Ab}	1.006 ± 0.014	1.013 ± 0.009

Table 4.13: Velocities of 20 Leonis using FB's (first section) and my (section b) data.

HJD 2440000+	Phase	V_{Aa} km/s	$(O-C)_{Aa}$ km/s	V_{Ab} km/s	$(O-C)_{Ab}$ km/s
(a)					
0989.0080	0.5039	− 67.20	+5.93	+132.20	+3.75
0990.8890	0.9575	+122.90	−0.69	− 70.70	+0.21
0992.9220	0.4478	− 69.80	−1.98	+122.90	−0.17
0992.9630	0.4577	− 64.50	+5.14	+129.60	+4.69
0996.8810	0.4025	− 55.60	−0.64	+110.00	−0.03
0996.9200	0.4119	− 57.00	+1.22	+115.60	+2.27
0998.8850	0.8858	+102.30	−0.14	− 52.40	−2.92
0998.9060	0.8909	+96.10	−8.40	− 50.50	+1.06
1000.8170	0.3517	− 39.40	−6.66	+ 87.80	+0.28
1000.8510	0.3599	− 45.30	−8.50	+ 90.50	−1.14
2087.7200	0.4614	− 68.20	+2.03	+125.40	−0.11
2087.8420	0.4908	− 75.30	−2.30	+123.10	−5.21
2089.7720	0.9563	+122.30	−1.08	− 74.20	−3.50
2091.7770	0.4398	− 67.40	−1.32	+118.40	−2.90
2093.8790	0.9467	+120.10	−1.47	− 70.00	−1.14
2141.6210	0.4598	− 74.40	−4.42	+124.90	−0.36
2143.6090	0.9392	+116.70	−3.22	− 67.60	−0.41
2143.8020	0.9858	+124.60	−2.14	− 75.50	−1.40
2145.7880	0.4647	− 77.80	−7.09	+127.00	+1.01
2344.9810	0.5006	− 76.40	−3.24	+127.60	−0.88
2346.9770	0.9820	+129.10	+2.60	− 71.20	+2.65
2437.7570	0.8738	+ 91.20	−6.08	− 43.40	+0.85
2440.0390	0.4241	− 58.50	+3.50	+117.50	+0.33
2443.9130	0.3584	− 44.60	−8.54	+ 88.80	−2.08
2504.6490	0.0050	+126.20	−0.89	− 73.60	+0.85
2506.6160	0.4794	− 69.00	+3.32	+134.10	+6.47

Table 4.13, continued.

HJD 2440000+	Phase	V_{Aa} km/s	$(O-C)_{Aa}$ km/s	V_{Ab} km/s	$(O-C)_{Ab}$ km/s
2558.6190	0.0200	+127.20	+0.86	− 73.90	−0.20
2560.6360	0.5065	− 78.50	−5.42	+129.70	+1.30
2564.6640	0.4778	− 68.30	+3.89	+130.30	+2.81
2712.0070	0.0100	+128.20	+1.26	− 71.60	+2.70
2763.9250	0.5302	− 76.60	−5.23	+134.00	+7.34
2856.7680	0.9195	+117.30	+2.70	− 60.20	+1.60
2856.7790	0.9222	+119.70	+4.30	− 61.10	+1.51
2856.7910	0.9251	+119.60	+3.36	− 63.70	−0.24
2856.8020	0.9277	+118.00	+1.02	− 62.00	+2.21
2856.8140	0.9306	+125.00	+7.23	− 61.80	+3.21
2856.8260	0.9335	+123.50	+4.98	− 62.20	+3.57
2856.8380	0.9364	+120.70	+1.45	− 64.80	+1.71
2856.8510	0.9395	+124.90	+4.91	− 64.60	+2.67
(b)					
7605.6760	0.1320	+ 87.70	−6.90		
7605.6760	0.1320			− 41.60	−0.07
7627.7010	0.4434	− 64.10	+2.80		
7627.7150	0.4468			+120.80	−2.06
7640.7050	0.5794	− 65.30	−4.34		
7640.7160	0.5820			+113.70	−1.59
7982.6670	0.0445	+114.00	−9.25		
7982.6830	0.0483			− 70.00	−0.14
7982.7130	0.0556	+114.70	−6.39		
7982.7260	0.0587			− 67.90	−0.22
7982.7530	0.0652	+109.00	−9.84		
7982.7650	0.0681			− 64.00	+1.35
7996.6730	0.4221	− 64.90	−3.51		

Table 4.13, continued.

HJD 2440000+	Phase	V_{Aa} km/s	$(O-C)_{Aa}$ km/s	V_{Ab} km/s	$(O-C)_{Ab}$ km/s
7996.6940	0.4271			+115.30	−2.73
7998.6690	0.9034	+ 99.60	−9.65		
7998.6850	0.9073			− 54.80	+2.96
8011.7070	0.0476	+116.90	−5.80		
8011.7250	0.0519			− 70.30	−1.15
8025.7430	0.4324	− 64.40	−0.14		
8025.7550	0.4353			+119.70	−0.50

Table 4.14: Velocities of the visual companion. The table includes both my and FB's data; a space separates FB's from the new data. It should be noted that in FB (1977), the velocity at HJD 2442346.977 was given as +08.4, and was assumed to be a typographical error. I have stated the value as +28.4.

HJD 2440000+	V km/s	HJD 2440000+	V km/s
0989.008	+33.3	2506.616	+30.0
0990.889	+30.3	2558.619	+31.7
0992.922	+25.4	2560.636	+29.9
0992.963	+31.1	2564.664	+28.6
0996.881	+27.2	2712.007	+22.6
0996.920	+30.8	2763.925	+30.8
0998.885	+35.0	2856.768	+19.3
0998.906	+26.2	2856.779	+20.8
1000.817	+20.7	2856.791	+22.4
1000.851	+20.8	2856.802	+24.4
2087.720	+29.0	2856.814	+28.2
2087.842	+28.0	2856.826	+28.0
2089.772	+26.4	2856.838	+26.2
2091.777	+32.6	2856.851	+19.9
2093.879	+23.9		
2141.621	+25.4	7605.676	+21.3
2143.609	+24.5	7627.731	+17.4
2143.802	+32.8	7640.726	+17.9
2145.788	+28.2	7982.670	+17.8
2344.981	+28.1	7982.739	+15.6
2346.977	+28.4	7982.798	+19.5
2437.757	+34.4	7996.719	+16.9
2440.039	+28.0	7998.699	+18.5
2443.913	+25.5	8011.715	+18.0
2504.649	+28.9	8025.766	+17.9

Upon inspection of Table 4.14, it is obvious that the new velocities are about 10 km/s less than FB's data. This could be due to a combination of two things: an instrumental difference, and a physical change in the system which we are able to detect. The residuals for the spectroscopic pair illustrate the velocity difference as well; the residuals for our data are nearly all substantially less than zero. An attempt was made to estimate how much of the velocity difference was due to the instruments, and how much occurred as a result of the change in the system.

Now, since we are dealing with the wide orbit, component A is the spectroscopic pair and component B is the visual companion, and it is assumed that all three stars are identical in mass. A change in the system as a whole manifests itself as a change in the radial velocity of B, and a change in the systemic (γ) velocity of A. Since A is twice as massive as B, its change will be half the change for B. Obviously, these two changes occur in opposite directions. The residuals may be used to estimate these quantities. The difference in the mean residual between FB's and our (denoted RS) spectroscopic data is due to a difference between the instruments (ΔV_I) and the change in the systemic velocity ($\Delta\gamma$) due to the orbital change. Thus, we may write

$$\overline{(O-C)}_{FB} - \overline{(O-C)}_{RS} = \Delta V_{I_A} + \Delta\gamma_A. \tag{4.5}$$

Similarly, the difference between FB's and our mean B velocities is due to the instrumental difference and the change in B's radial velocities due to orbital motion, which gives us

$$\overline{V}_{B_{FB}} - \overline{V}_{B_{RS}} = \Delta V_{I_B} + \Delta V_{*_B}. \tag{4.6}$$

However, the explanation at the start of the paragraph implies that

$$\Delta V_{I_A} = \Delta V_{I_B} \tag{4.7}$$

$$2\Delta\gamma_A = -\Delta V_{*_B}. \tag{4.8}$$

Upon calculation, it was found that the mean residuals and B velocities were 0.31, −1.27, 27.38 and 18.08 km/s, for FB's and our data, respectively. These then led to $\Delta V_{I_B} = \Delta V_{I_A} = 4.15$ km/s, $\Delta\gamma_A = -2.57$ km/s and $\Delta V_{*_B} = 5.14$ km/s. Thus, an adjustment of $\Delta\gamma_A + \Delta V_{I_A} = 1.58$ km/s was added to our velocities to bring them to the system and epoch of FB's observations, and the orbit was solved again using the corrected velocities. The corrected orbital elements may be found in Table 4.15. Figure 4.3 is the radial velocity curve using the corrected velocities. FB's data are designated by open circles; the filled circles pertain to our data.

The velocity change of the visual companion due to the orbital change for the relative orbit of the wide pair is thus given as $\Delta\gamma_A - \Delta V_{*_B} = 7.72$ km/s. Implications of this will be discussed in the final section of this chapter.

Table 4.15: Revised orbital elements for 20 Leonis, obtained after correcting the new velocities by 1.58 km/s.

Parameter	Corrected Value
P	4.1467465 ± 0.0000088 days
T_0	2442094.100 ± 0.007 HJD
K_{Aa}	100.10 ± 0.74 km/s
K_{Ab}	101.31 ± 0.52 km/s
γ	27.31 ± 0.33 km/s
$a_{Aa} \sin i$	5.708 ± 0.042 Gm
$a_{Ab} \sin i$	5.777 ± 0.029 Gm
$M_{Aa} \sin^3 i$	1.77 ± 0.02 $M_\odot$
$M_{Ab} \sin^3 i$	1.75 ± 0.03 $M_\odot$
M_{Aa}/M_{Ab}	1.012 ± 0.009

Figure 4.3: Radial velocity curve using the orbital solution for $e = 0.0$, and revised velocities. Phases are computed from time of nodal passage.

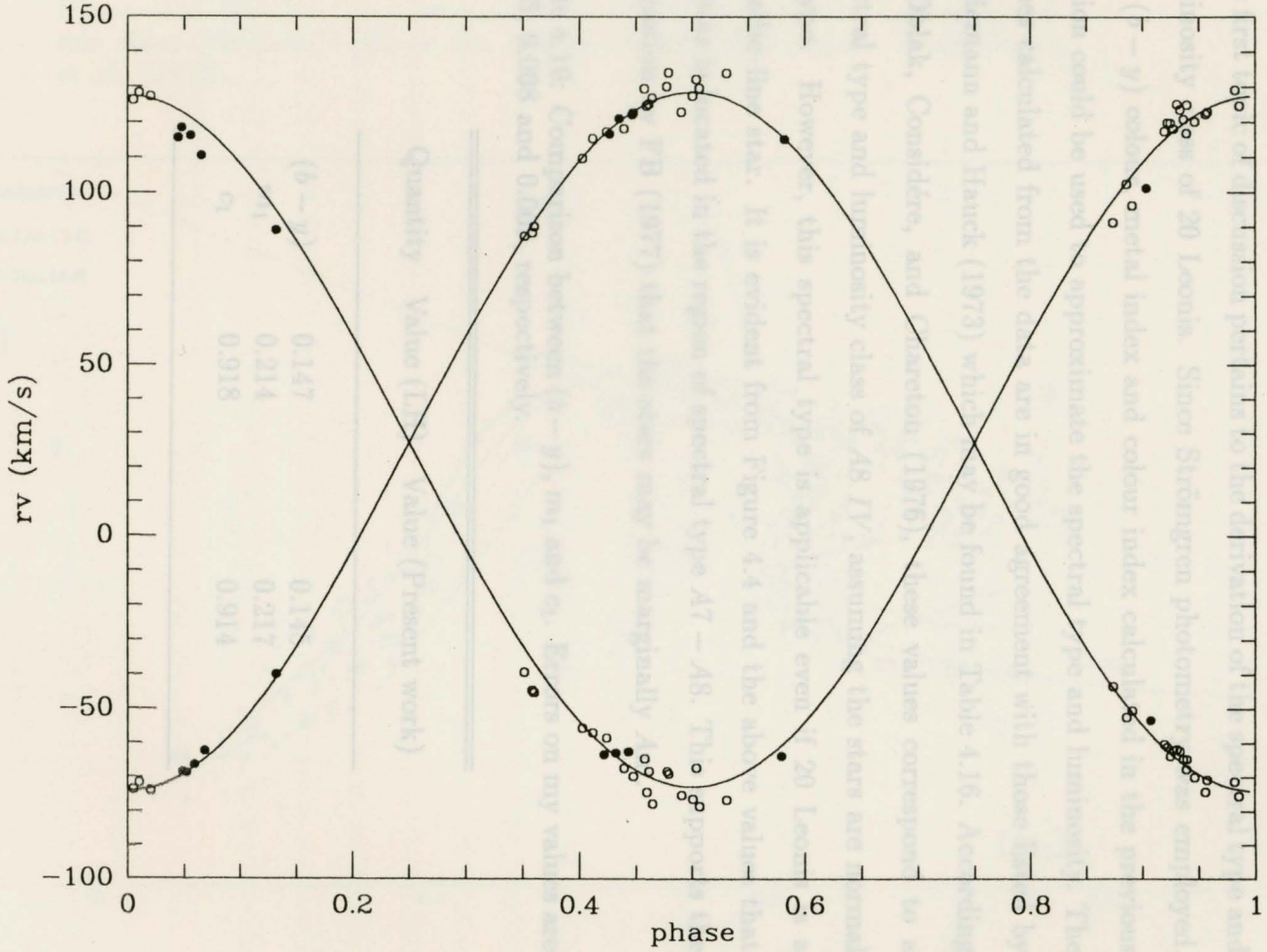

4.6 Discussion

The first topic of discussion pertains to the derivation of the spectral type and luminosity class of 20 Leonis. Since Strömgren photometry was employed, the $(b-y)$ colour, metal index and colour index calculated in the previous section could be used to approximate the spectral type and luminosity. The values calculated from the data are in good agreement with those listed by Lindemann and Hauck (1973) which may be found in Table 4.16. According to Oblak, Considére, and Chareton (1976), these values correspond to a spectral type and luminosity class of $A8\ IV$, assuming the stars are normal A–type. However, this spectral type is applicable even if 20 Leonis is a metallic–line star. It is evident from Figure 4.4 and the above values that the star is located in the region of spectral type $A7 - A8$. This supports the suggestion by FB (1977) that the stars may be marginally Am.

Table 4.16: Comparison between $(b-y)$, m_1 and c_1. Errors on my values are 0.005, 0.008 and 0.009, respectively.

Quantity	Value (LH)	Value (Present work)
$(b-y)$	0.147	0.145
m_1	0.214	0.217
c_1	0.918	0.914

Figure 4.4: The $[m_1]$–$[c_1]$ diagram for the metallic, peculiar and emission–line stars. 20 Leonis falls in the metallic–line A star region. From Oblak, et al. (1976).

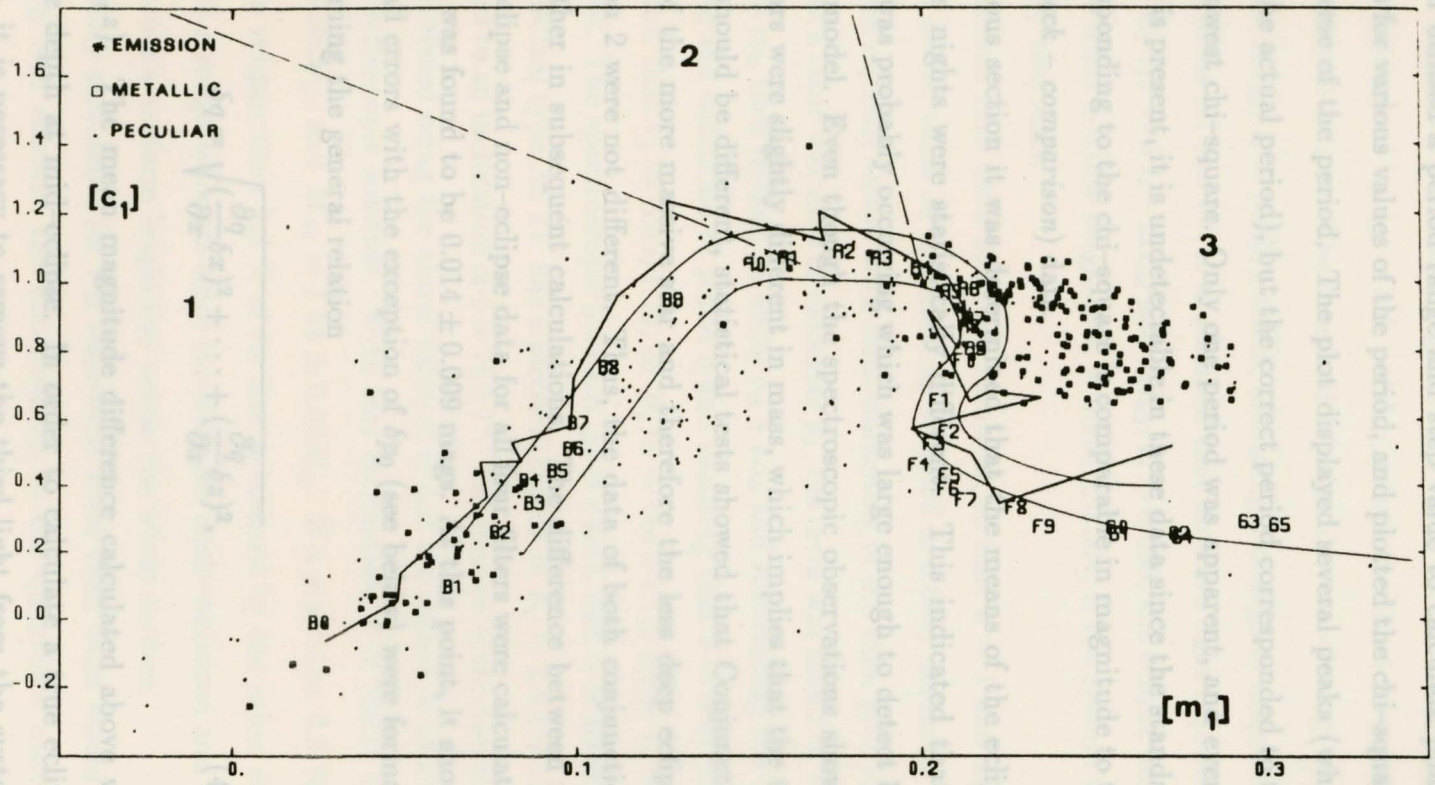

The next topic of discussion involves the δ Scuti variation. The period–finding program utilised a period range and step value to calculate phases and chi–squares for various values of the period, and plotted the chi–squares against the inverse of the period. The plot displayed several peaks (which were aliases of the actual period), but the correct period corresponded to the peak with the lowest chi–square. Only one period was apparent, and even if a second period is present, it is undetectable in these data since the standard deviation corresponding to the chi–square is comparable in magnitude to the error in the (*check - comparison*) data.

In the previous section it was determined that the means of the eclipse and non–eclipse nights were statistically different. This indicated that a grazing eclipse was probably occurring which was large enough to detect but too shallow to model. Even though the spectroscopic observations showed that the two stars were slightly different in mass, which implies that the two eclipse depths should be different, statistical tests showed that Conjunction 1 (the eclipse of the more massive star and therefore the less deep eclipse) and Conjunction 2 were not different. Thus, the data of both conjunctions were used together in subsequent calculations. The difference between the means for the eclipse and non–eclipse data for all four filters were calculated, and an average was found to be 0.014 ± 0.009 mags. At this point, it should be noted that all errors with the exception of δp_0 (see below) were formally calculated assuming the general relation

$$\delta q = \sqrt{(\frac{\partial q}{\partial x}\delta x)^2 + \cdots + (\frac{\partial q}{\partial z}\delta z)^2}, \tag{4.9}$$

for $q = q(x, ..., z)$. The mean magnitude difference calculated above was taken to be the depth at mid–eclipse. In order to calculate a true eclipse depth, however, it is necessary to remove the third light from the system.

Please refer to Figure 4.5 for the system's geometry. The intensity of the light from the system in situation I may be given by $I_I = 3\ I_*$. In situation II, the intensity is represented by $I_{II} = 3\ I_* - \Delta I_{ecl}$, where the third term refers to the light lost due to eclipse. The standard relation $\Delta m = -2.5 \log(\frac{I_{II}}{I_I})$ is used to determine $\Delta I_{ecl}/I_* = 0.038 \pm 0.008$, assuming a change in magnitude of 0.014. In situations III and IV, it is assumed that no third light is present. Taking $I_{III} = 2\ I_*$, $I_{IV} = 2\ I_* - \Delta I_{ecl}$ and $\Delta I_{ecl}/I_* = 0.038$, the eclipse depth would have been 0.021 ± 0.004 mags, or $l_0 = 0.981 \pm 0.004$, if the system was composed of only two stars.

Now, let's assume that both stars are identical, so that k = 1 and $L_s = L_g = 0.5$. The above value of l_0 yields $\alpha_0 = 0.038 \pm 0.008$, assuming no error in L_g. Irwin's (1962) tables with limb–darkening of 0.5 then give $p_0 = 0.78 \pm 0.03$. Since a table was used to calculate p_0, the error was found by first deriving p_0 from α_0, then finding p_0 using $\alpha_0 + \delta\alpha_0$ and subtracting the two results. By using the definition of p and δ and realizing that $\theta = 0$ at mid–eclipse, it is found that $r_g = \cos i/1.78$, or $R_g/a = \cos i/1.78$, since r_g is in terms of the orbit. The spectroscopic solution gives $a \sin i$, and it is assumed that a star of spectral type *A8 IV* has a physical radius of $R_g = 2.5 \pm 0.1 R_\odot$. These values lead to an inclination of $i = 75 \pm 1°$. The masses of the two stars may now be calculated using the above value of i, and the values of $M \sin^3 i$ given by the spectroscopic solution. With this inclination, it is found that $M_{Aa} = 1.96 \pm 0.04 M_\odot$, and $M_{Ab} = 1.94 \pm 0.05 M_\odot$. If a star loses 3.8 % of its luminosity in eclipse, then 3.8 % of its disk is covered by the other star. Of course, this is a rough estimate since the stars are limb–darkened and the calculation assumes a uniform brightness across the whole surface.

The uncertainty calculated for i is somewhat lower than what would be expected, taking into account the uncertainties in the quantities used to

Figure 4.5: The system geometry. Shaded areas refer to the loss of light from the system.

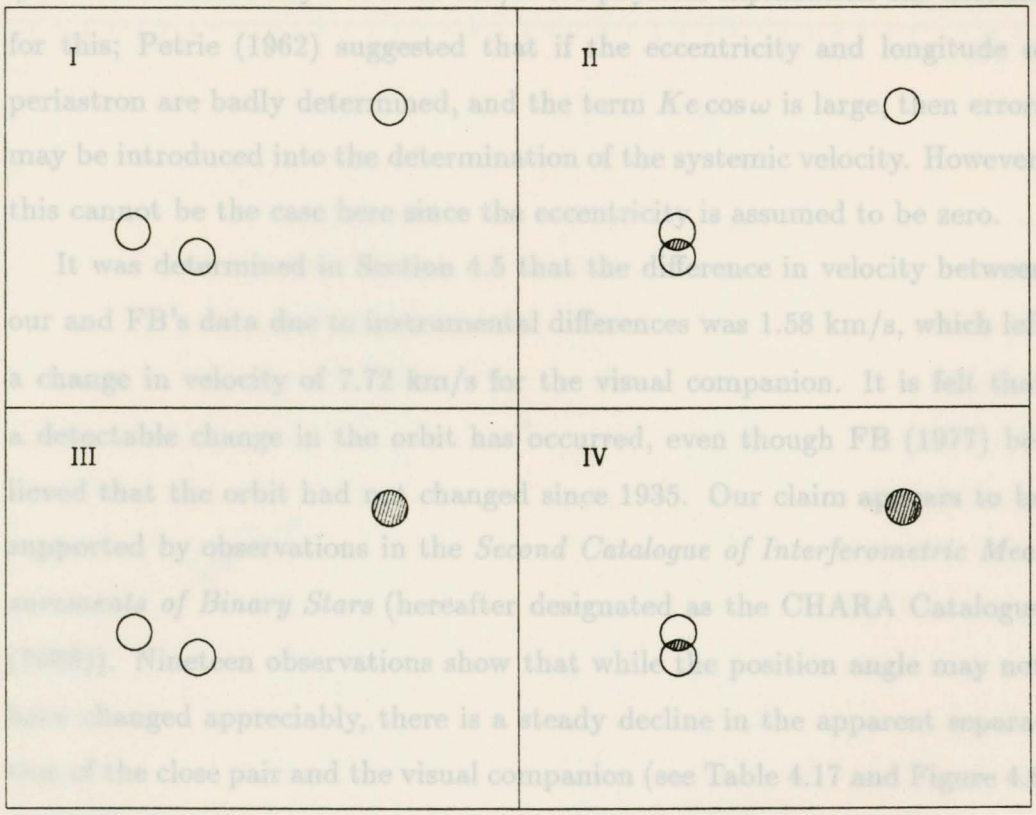

determine the inclination. It is suspected that the approach taken is not entirely valid in this case, since a trigonometric function is involved. The tangent is defined such that at angles close to 90°, the uncertainties in the quantities may be varied quite a bit and not affect the final result very much.

A short discussion of the spectroscopic data is in order. Firstly, when the orbits of the two stars were solved individually, it was noticed that the γ velocities differed by about 10 km/s. No physical explanation can account for this; Petrie (1962) suggested that if the eccentricity and longitude of periastron are badly determined, and the term $Ke\cos\omega$ is large, then errors may be introduced into the determination of the systemic velocity. However, this cannot be the case here since the eccentricity is assumed to be zero.

It was determined in Section 4.5 that the difference in velocity between our and FB's data due to instrumental differences was 1.58 km/s, which left a change in velocity of 7.72 km/s for the visual companion. It is felt that a detectable change in the orbit has occurred, even though FB (1977) believed that the orbit had not changed since 1935. Our claim appears to be supported by observations in the *Second Catalogue of Interferometric Measurements of Binary Stars* (hereafter designated as the CHARA Catalogue (1988)). Nineteen observations show that while the position angle may not have changed appreciably, there is a steady decline in the apparent separation of the close pair and the visual companion (see Table 4.17 and Figure 4.6 for these data).

These new data suggest that the relative orbit is highly inclined, and the fact that we are now seeing evidence of orbital motion implies that the orbit is probably eccentric and the visual companion may be approaching periastron. Unfortunately, the old data were not available, so quantitative results for this orbit cannot be determined. However, if this star is indeed

approaching periastron, it will be worthwhile to observe the system over the next couple of decades. By that time, enough of the orbit may have been covered to permit a tentative solution.

Figure 4.6: Partial visual orbit for 20 Leonis, based on Table 4.15. The black dot designates the location of the spectroscopic pair. The data have been converted to cartesian coordinates for the purpose of plotting the orbit.

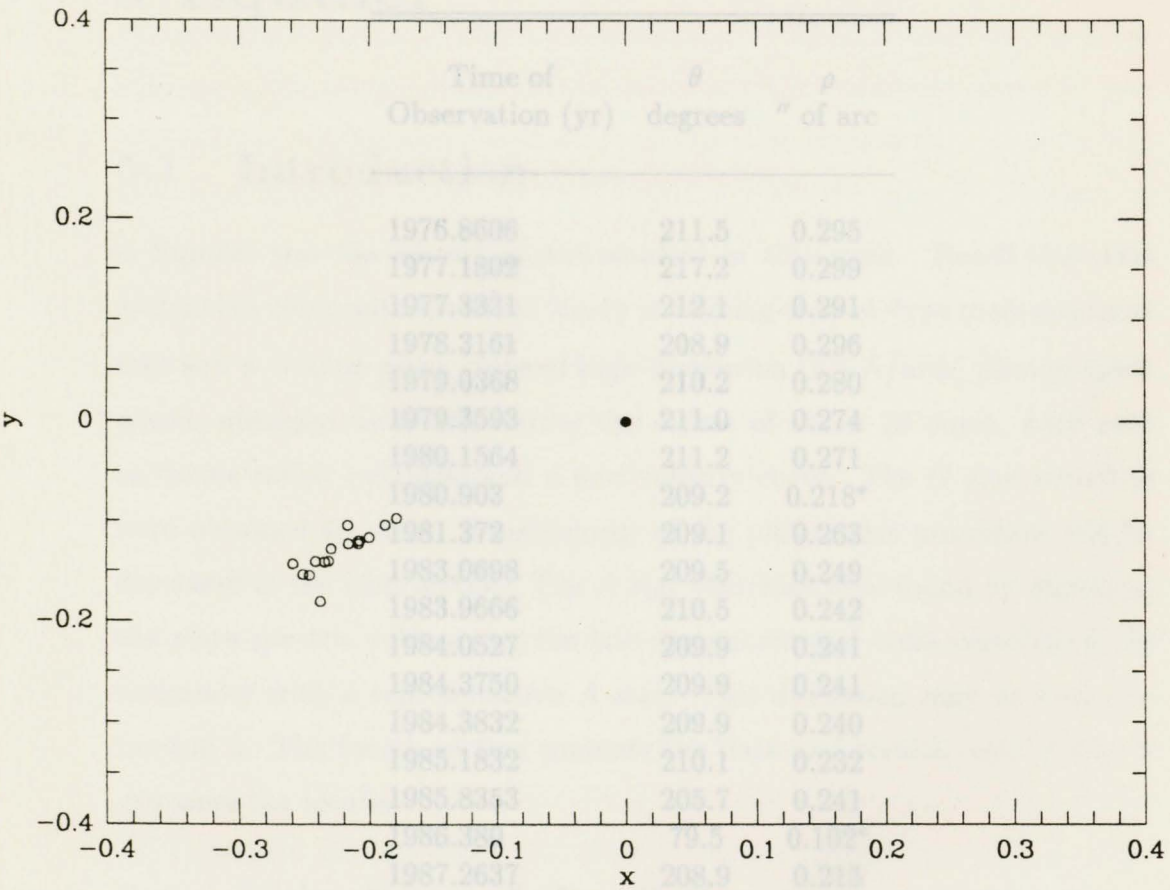

Table 4.17: Interferometric measurements of the visual companion of 20 Leonis. Two measurements have been omitted from the corresponding plot, since they appeared highly incorrect. They have been marked in the table with a *. θ is the position angle, while ρ is the projected separation. From the CHARA Catalogue (1988).

Time of Observation (yr)	θ degrees	ρ " of arc
1976.8606	211.5	0.295
1977.1802	217.2	0.299
1977.3331	212.1	0.291
1978.3161	208.9	0.296
1979.0368	210.2	0.280
1979.3593	211.0	0.274
1980.1564	211.2	0.271
1980.903	209.2	0.218*
1981.372	209.1	0.263
1983.0698	209.5	0.249
1983.9666	210.5	0.242
1984.0527	209.9	0.241
1984.3750	209.9	0.241
1984.3832	209.9	0.240
1985.1832	210.1	0.232
1985.8353	205.7	0.241
1986.380	79.5	0.102*
1987.2637	208.9	0.215
1988.2521	208.5	0.204

Chapter 5

α Equulei

5.1 Introduction

α Equulei was the second system studied in this work. Recall that this system is a composite spectrum binary consisting of an A–type main sequence star and a G–type giant. Several high–dispersion (2.4 Å/mm) photographic plates, obtained by Scarfe during the course of about 20 years, were used to derive radial velocities and a new velocity curve. The G star velocities were obtained by direct measurement of the plates; this procedure will be discussed in the next section. The A star velocities were found by digitizing the plate spectra, subtracting the late component and cross–correlating the remainder with a representative A star. This discussion may be found in Section 3. The fourth section presents the data and results, and Section 5 discusses the results.

5.2 Velocities of the G Star

The G–type component of α Equulei could be measured directly since there are many strong metal lines which are relatively free of A star contamination. The ARCTURUS measuring machine, which was developed at the DAO, was used to determine the radial velocities of the G component. This machine is

based on an Abbè comparator, a measuring instrument which consists of two microscopes and a travelling plate bed. One microscope is used to scan the plate while the other views a ground–glass scale which is fixed to the plate bed. The positions of arc and stellar lines on the plate are measured with respect to a location on the plate corresponding to the approximate centre of the wavelength region being scanned.

The ARCTURUS machine removes some of the tedium involved in measuring a plate with the Abbè comparator; instead of looking at the plate through a microscope and trying to determine the centre of a line, the user views on an oscilloscope two tracings of the plate transmission near to that line. One tracing is in the forward direction while the other is reversed. A computer terminal displays the radial velocity table containing wavelengths and positions of carefully chosen arc and stellar lines, and rVs factors (the number of km/s in one mm on the plate) for the stellar lines. The positions and rVs factors are calculated for zero velocity and an assumed dispersion, directly from the spectrograph properties. The user measures each line in the table by superposing the two tracings; the computer encodes and records the position of the plate bed. It is fairly obvious that the ARCTURUS machine speeds up the measuring procedure, and yields results which are more accurate than those found by the Abbè comparator alone.

The program then computes the observed and heliocentric velocities for the plate via the following steps. Since the plate dispersion is often slightly different from that on which the velocity table is based, the positions of the comparison lines will differ from those listed in the table. This discrepancy is remedied by plotting the differences between the measured and tabulated positions against the measured positions, for all comparison lines. A polynomial is fitted to the data, and the resulting correction curve is applied to each stellar line measurement in order to correct the dispersion. Next,

the differences between the corrected positions and those in the table for the stellar lines are obtained and multiplied by the appropriate rVs factor to get the radial velocity for each measured stellar line. Finally, the mean and standard deviation of the individual velocities are calculated, giving the plate, or observed, velocity.

Heliocentric velocities, or velocities with respect to the sun, are determined by removing the effects of the observer's motion caused by the rotation and revolution of the earth. The contribution to the radial velocity from the latter effect is the most important, and is given by

$$V_{\oplus} = b \sin(\lambda_{\odot} - \lambda_{\star}) + c \tag{5.1}$$

where

$$b = -\frac{2\pi a \cos \beta_{\star}}{P\sqrt{1-e^2}} \tag{5.2}$$

$$c = -be \sin(\omega - \lambda_{\star}) \tag{5.3}$$

and P is the earth's orbital period, e is the eccentricity of the earth's orbit, a is the semimajor axis of the earth's orbit, ω is the longitude of perihelion of the earth, $\lambda_{\star}$ and $\beta_{\star}$ are the ecliptic coordinates of the star, and $\lambda_{\odot}$ is the sun's longitude at the time of observation. The rotational, or diurnal correction is quite minor, and is given by

$$V_d = V_r \cos \delta \sin H \tag{5.4}$$

where

$$V_r = V_e(1 + \frac{b^2}{a^2} \tan^2 \phi)^{-1/2} \tag{5.5}$$

is the rotational velocity of the earth's surface at the latitude of the observatory (ϕ), δ is the star's declination, H is the hour angle at the time of

observation, V_e is the earth's equatorial velocity, and a and b are the equatorial and polar radii, respectively. These two quantities are calculated and subtracted from the observed velocity to give the heliocentric velocity. Other corrections such as that to the earth–moon barycentre (centre of mass) and solar system barycentre are not required. Highly accurate radial velocity studies must correct for these two effects, but in this case, the corrections would be less than the uncertainties of the measured velocities.

35 V plates were measured with ARCTURUS. The V (violet) plates cover a wavelength range from about 4190 to 4630 Å, and at these wavelengths, contamination from the A star is not much of a problem. Errors in the velocities were less than 1.0 km/s; these accurate determinations helped a great deal in the subsequent analysis of the orbit.

5.3 Analysis of the *A* Star

The velocities of the A–type component were obtained in an entirely different manner. Direct measurement of the lines was not feasible since there were few lines strong enough to be visible with ARCTURUS, and contamination from the G star was a major problem. The alternative procedure involved taking the steps outlined in the first paragraph of this chapter, and using the U, or ultraviolet plates (wavelengths from about 3700 to 4170 Å), since the A star's presence is more apparent in this region. It should be noted that 26 U plates were used in this procedure.

The DAO's PDS microdensitometer was used to digitize the spectra. This instrument utilizes a high speed photometer to measure the plate density, and a computer to control the scanning and record the density at various positions on the photographic plate. Five files for each plate are written to magnetic tape. The first two files contain the scans of the density of the calibration

wedges at two plate locations, while the next contains the clear plate density recorded across the length of the plate. The fourth file is comprised of each arc spectrum, while the fifth consists of the two scans of the stellar spectrum.

The digitized spectra were reduced to a form suitable for cross–correlation using the IRAF (Image Reduction and Analysis Facility) package and a SUN workstation, again at the DAO. This package of computer programs was developed by NOAO (National Optical Astronomy Observatories) and is used to reduce various types of astronomical data. A brief description of the steps required will be presented here; refer to Appendix A for a discussion complete with plots and IRAF task names.

The first step in reducing the spectra involved conversion from a density to an intensity scale. The logs of the exposure values and the mean densities of the calibration wedges were plotted, and a polynomial was fitted to the data. This characteristic curve was then applied to the stellar spectra to transform their density readings into intensities. The clear plate reading was subtracted from each wedge and the stellar spectrum before any plotting or transforming occurred. Next, the arc lines were assigned their corresponding wavelengths, and a dispersion function was found from the wavelengths and pixel positions of the lines. This equation was used to assign a wavelength scale to the stellar spectra. Finally, a function was fitted to the continuum, and the spectrum was divided by that function.

At this point, it was necessary to subtract the late–type spectrum from the spectrum of α Equulei. For an excellent detailed description of spectral subtraction, see Griffin (1986). In this procedure, it is very important to match as closely as possible the spectral type and luminosity class of the *G* component with a single *G* star, so that the correct amount of all the lines is subtracted. In the ideal case, all the late–type absorption lines should vanish at the same time. This rarely happens, however, since it is extremely

difficult to determine exactly the luminosity and spectral type of the late type component, and no two stars have spectra exactly alike. Any residual *G* star contamination will affect the cross–correlation peak, resulting in an incorrect velocity determination and a large uncertainty. Since it is difficult to find a near–to–perfect match, two *G* stars were used in the procedure, and the results were compared.

Before subtraction could commence, it was necessary to align as exactly as possible the spectra of the late component and the single star. If the two spectra do not coincide, or if there are differences in the dispersion, then subtraction is ineffective. In order to align the spectra of α Equulei and the single *G* star, the differences in the positions of several lines throughout the wavelength range were recorded to three decimal places, an average difference was found, and the *G* component was shifted by this amount. Fractions, in increments of 5 percent of the spectrum of the single *G* star, were then subtracted from α Equulei's spectrum. It was possible to ascertain when the correct amount had been subtracted by visually inspecting the resulting spectra. As more and more of the late–type spectrum was subtracted, the cool star's absorption lines became progressively weaker, until they virtually disappeared. Further increments resulted in the appearance of emission–type features.

The remaining spectrum was smoothed (to decrease noise) and cross–correlated against a smoothed template star, in order to obtain the radial velocities. The cross–correlation technique follows that of Tonry and Davis (1979). The object and template spectra are transformed to Fourier space and the object transform is multiplied by the complex conjugate of the template transform. The result is transformed back to real space, producing a normalized correlation function, the peak of which is at a lag corresponding to the shift between the two spectra. A Gaussian is then fit to the correlation

function in order to determine the exact shift and thus the observed velocity of the object star. Determination of the heliocentric velocity was the last step.

5.4 Data and Results

The standard deviations in the radial velocities of the G component ranged from 0.30 to 0.85 km/s; the average deviation was 0.46 km/s. The A velocities were not as accurate, however. The two G stars used in the subtraction are listed in Table 5.1. It was found that subtraction using β Bootis produced cleaner subtracted spectra, and yielded consistently higher and "more Gaussian" correlation peaks than did 24 Ursae Majoris. Thus, the former was used for all the α Equulei spectra. The template star was 68 Tauri, an A–type radial velocity standard star. Its heliocentric velocity was taken to be 36.7 km/s, found by applying the heliocentric correction to the observed velocity which was derived by cross–correlating the star with an inverted iron arc spectrum. Standard deviations of the velocities resulting from the cross–correlation ranged from 0.31 to 1.27 km/s, with an average of 0.61 km/s. However, it is felt that the true error is probably more on the order of 2 or 3 km/s since there were uncertainties in every step of the reduction, not all of the G star could be subtracted, and the inclusion or omission of certain lines in the correlation changed the calculated velocity by as much as 2 km/s in some cases.

Orbital elements were calculated for each component, using the same software as for 20 Leonis and assuming an eccentric orbit. Standard errors of an observation of unit weight were calculated as 0.27 and 2.39 km/s for the G and A star, respectively. The inverse squares of the above values were used to weight the observations in preparation for a simultaneous solution. Note

Table 5.1: The template star used in the cross–correlation, and the standard stars used in the subtraction of the G component. Coordinates are for an equinox and equator of 2000.0.

HD	RA (h m s)	DEC (° ′ ″)	Sp. Type
27962 (68 Tauri)	04 25 29	+17 55 41	*A2 V/A6 V**
82210 (24 UMa)	09 34 29	+69 49 49	*G2 IV*
133208 (β Boo)	15 01 57	+40 23 26	*G8 III*

*Note: 68 Tauri has a spectral type of *A2* according to its hydrogen lines, but appears later when one considers its strong, sharp metallic lines.

that since the A star carries such little weight (0.01, as compared to 1.0 for the G star), the orbital elements except for K_A are being determined almost exclusively from the G star observations. The individual solutions yielded eccentricities with uncertainties as large as the eccentricities themselves. Thus, $e = 0$ was adopted and a simultaneous circular solution was calculated.

Table 5.2 contains, for the sake of comparison, the orbital elements obtained using a circular solution and our new data, and elements from Pike's data. Pike's velocities are listed in Appendix B.

Table 5.2: Orbital elements of Alpha Equulei obtained by solving for both stars simultaneously. The results are from our data (I), and Pike's data (II). In both cases, the orbit is assumed to be circular. Note: Gm = gigameters.

Parameter	I	II
P	98.803 ± 0.004 days	100.04 ± 0.32 days
T_0	2443614.31 ± 0.08 HJD	2441738.51 ± 0.52 HJD
K_G	16.236 ± 0.065 km/s	15.40 ± 0.65 km/s
K_A	18.65 ± 0.75 km/s	19.0 ± 1.3 km/s
γ	-16.617 ± 0.045 km/s	-18.37 ± 0.38 km/s
$a_G \sin i$	22.06 ± 0.09 Gm	21.19 ± 0.90 Gm
$a_A \sin i$	25.3 ± 1.0 Gm	26.1 ± 1.8 Gm
$M_G \sin^3 i$	$0.233 \pm 0.019 M_\odot$	$0.233 \pm 0.035 M_\odot$
$M_A \sin^3 i$	$0.203 \pm 0.009 M_\odot$	$0.189 \pm 0.021 M_\odot$
M_G/M_A	1.149 ± 0.046	1.232 ± 0.099

Table 5.3: Velocities and residuals from a simultaneous solution of our data for α Equulei. The orbit is assumed to be circular.

HJD 2440000+	Phase	V_G km/s	$(O-C)_G$ km/s	V_A km/s	$(O-C)_A$ km/s
0429.9343	0.7705	−14.04	+0.49	−19.6	−0.6
0441.8721	0.8913	− 3.89	+0.13	−30.2	+0.9
0499.7688	0.4773	−32.56	+0.13		
0723.9843	0.7466	−16.71	+0.26		
0810.8061	0.6253	−28.20	−0.13		
0829.7816	0.8174	−10.01	−0.06	−23.5	+0.8
0856.7576	0.0904	− 2.77	+0.16	−30.8	+1.6
0888.6509	0.4132	−30.24	+0.26	− 2.4	−1.8
1144.9045	0.0068	− 0.30	+0.10		
1162.8538	0.1884	−10.10	+0.39	−21.1	+2.6
1897.9285	0.6282	−27.86	+0.00	− 2.7	+1.0
1904.8245	0.6980	−22.01	−0.19		
1909.8783	0.7492	−16.99	−0.29	−17.7	−1.2
2234.9358	0.0391	− 1.04	−0.17	−30.3	+4.4
2242.8713	0.1195	− 4.87	−0.13	−30.6	−0.3
2253.8498	0.2306	−14.67	−0.03	−19.5	−0.6
2269.8386	0.3924	−29.45	−0.17	− 2.8	−0.7
2273.8887	0.4334	−31.66	−0.21	− 0.9	−1.3
2280.8495	0.5038	−32.97	−0.12	+ 0.2	−1.9
2305.7794	0.7562	−16.08	−0.09		
2318.7943	0.8879	− 4.47	−0.22	−29.4	+1.4
2354.6330	0.2506	−16.74	−0.06	−18.7	−2.1
2657.8714	0.3197	−23.76	−0.26	−12.6	−3.9
2661.8040	0.3595	−27.09	−0.16	− 5.1	−0.3
2681.8454	0.5624			+ 3.7	+3.1
2681.8739	0.5627	−31.81	−0.20	+ 1.4	+0.8
2752.5405	0.2775			−17.3	−3.9
2935.9715	0.1344	− 5.35	+0.49		
2975.9432	0.5390	−32.24	+0.13		
3088.6154	0.6793	−23.73	−0.14		

Table 5.3, continued.

HJD 2440000+	Phase	V_G km/s	$(O-C)_G$ km/s	V_A km/s	$(O-C)_A$ km/s
3110.5599	0.9014	− 4.09	−0.69		
3301.9573	0.8386	− 8.22	−0.18	−28.1	−1.7
3312.9492	0.9499	− 1.59	−0.41	−36.6	−2.2
3347.8741	0.3033	−21.89	+0.07	− 8.3	+2.2
5932.7870	0.4656	−32.41	+0.07		
6288.8050	0.0689	− 1.56	+0.32	−39.2	−5.6
7042.7640	0.6998	−21.00	+0.65		
7375.9060	0.0716			−36.1	−2.7

Figure 5.1: Radial velocity curve for the simultaneously solved orbit, using only the new data. Key: o = G, • = A.

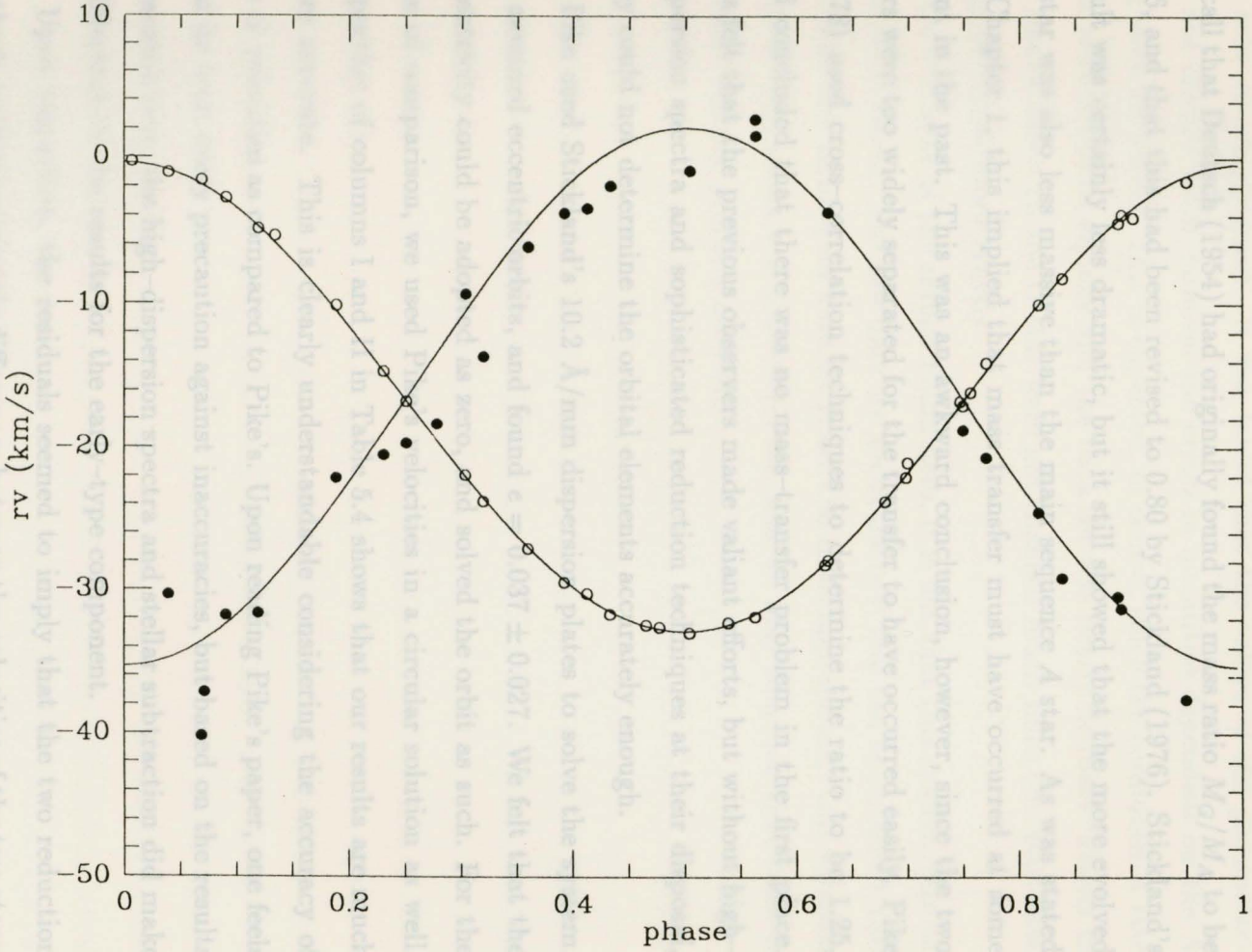

5.5 Discussion

Recall that Deutsch (1954) had originally found the mass ratio M_G/M_A to be 0.26, and that this had been revised to 0.80 by Stickland (1976). Stickland's result was certainly less dramatic, but it still showed that the more evolved G star was also less massive than the main sequence A star. As was stated in Chapter 1, this implied that mass transfer must have occurred at some point in the past. This was an awkward conclusion, however, since the two stars were too widely separated for the transfer to have occurred easily. Pike (1978) used cross–correlation techniques to determine the ratio to be 1.25, and concluded that there was no mass–transfer problem in the first place. It is felt that the previous observers made valiant efforts, but without high–dispersion spectra and sophisticated reduction techniques at their disposal, they could not determine the orbital elements accurately enough.

Pike used Stickland's 10.2 Å/mm dispersion plates to solve the system. He assumed eccentric orbits, and found $e = 0.037 \pm 0.027$. We felt that the eccentricity could be adopted as zero, and solved the orbit as such. For the sake of comparison, we used Pike's velocities in a circular solution as well. Inspection of columns I and II in Table 5.4 shows that our results are much more accurate. This is clearly understandable considering the accuracy of our G velocities as compared to Pike's. Upon reading Pike's paper, one feels that he took every precaution against inaccuracies, but based on the results presented here, the high–dispersion spectra and stellar subtraction did make a difference in the results for the early–type component.

Upon inspection, the residuals seemed to imply that the two reduction methods yielded systematic differences between the velocities of the two stars. Although a zero point correction was not calculated and applied to the velocities, it was estimated that it could amount to about 1 km/s.

Our and Pike's data were combined and the orbit was solved again, for the sake of completeness. It was found that the values of the parameters did not change much, however the errors in quantities dependent on the *A* star were decreased. This is expected, of course, since the combined *A* star data were weighted equally and the data set was nearly doubled. Errors in the results based on the *G* star were not changed much since our data were weighted much more heavily.

On the basis of the results found here, it is felt that this system may be considered solved. The new data are about the best that can be obtained, and the reduction techniques used on it are the most appropriate. Our solution confirms that which was found by Pike, and we may conclude that there is no mass transfer problem after all.

Chapter 6

Conclusion

In conclusion, it is felt that the goals of this work have been attained. The study of 20 Leonis proved to be quite fruitful; the Strömgren photometry confirmed the spectral type of 20 Leonis as $A8\ IV$ and the possibility that it is marginally Am. The δ Scuti behavior was very apparent but only one period of 0.0826 days could be derived from the data. The difference in the mean light levels between the eclipse and non–eclipse nights signified a grazing eclipse, too shallow to produce a recognizable light curve but apparent enough to allow the calculation of an inclination. It was found that $i = 75 \pm 1$ degrees. This is an important determination since the masses of the two stars are now known more accurately.

A new orbital solution for the close pair of 20 Leonis was calculated from the combination of 10 new radial velocities and velocities obtained by FB (1977) (see Table 4.14). It was also interesting to see that our radial velocities of the third star were consistently lower than those of FB. We attributed this to a systematic difference between our and FB's velocities as well as to a real observable change in the system, and estimated the contributions of these as 1.58 km/s and 7.72 km/s, respectively. Even though FB had suggested that the system had not changed position since 1935, we were able to tentatively show that the orbit is highly inclined and possibly eccentric, and that the

third star is approaching periastron.

The composite spectrum binary α Equulei was analysed in order to solve a potential problem with the mass ratio. Previous studies had given the mass ratio M_G/M_A such that the more evolved primary star was also less massive than the non–evolved secondary. However, it was felt that this was due mostly to poor data and inappropriate reduction techniques. The most recent previous study (Pike, 1978) gave the mass ratio as $M_G/M_A = 1.25$, which meant that there was no mass ratio problem after all. In order to verify this, 35 V photographic plates of α Equulei were reduced using the DAO's ARCTURUS measuring machine, to obtain radial velocities of the G star. The A star velocities were obtained by scanning 26 U photographic plates and reducing the resulting images with IRAF. It was felt that by subtracting the G component, smoothing the spectra to eliminate further noise, and obtaining the velocities via cross–correlation techniques, better velocities of the A star could be obtained. It was found that our data and subsequent orbital solution were much improved over the previous solutions (see Table 5.2). We found the mass ratio M_G/M_A to be 1.15, thus verifying Pike's result.

The α Equulei system is considered solved, since further observation or analysis would not substantially improve the orbital elements. However, better photometric data of 20 Leonis could prove beneficial in several respects. For example, fast photometry would result in a longer data string which could reveal another δ Scuti period, and more accurate photometry could verify or negate the possibility of eclipses. In a different vein, long–term observations of the visual companion using interferometric techniques would provide more insight into the visual orbit, and yield a possible preliminary solution.

References

Aitken, R. G. 1935, *The Binary Stars* (New York: McGraw–Hill).

Barnes, T. G., Fekel, F. C., Moffett, T. J., 1977. *Pub. Astron. Soc. Pac.* **89**, 658.

Batten, A. H. 1973, *Binary and Multiple Systems of Stars* (Oxford: Pergamon Press).

Breger, M., 1979. *Pub. Astron. Soc. Pac.* **91**, 1.

Crawford, D. L., 1966, in *Spectral Classification and Multicolour Photometry, IAU Symp.* **24**, eds. K. Lodén, L. O. Lodén, and U. Sinnerstad.

Crawford, D. L., and Barnes, J. V., 1970. *Astron. J.* **75**, 978.

Deutsch, A. J., 1954. *Pub. Astron. Soc. Pac.* **66**, 58.

Elliott, J. E., 1974. *Astron. J.* **79**, 1082.

Fekel, F. C. and Bopp, B. W., 1977. *Pub. Astron. Soc. Pac.* **89**, 216.

Fletcher, J. M., et al., 1982. *Pub. Astron. Soc. Pac.* **94**, 1017.

Frolov, M. S., 1975, in *Pulsating Stars*, B. V. Kukarkin, ed. (Jerusalem: Keter Pub. House).

Graham, J. A., 1982. *Pub. Astron. Soc. Pac.* **94**, 244.

Griffin, R. and Griffin, R., 1986. *J. Astrophys. Astron.* **7**, 195.

Hall, D. S., and Genet, R. M., 1982, *Photoelectric Photometry of Variable Stars*, Pub. by International Amateur–Professional Photoelectric Pho–

tometry.

Heintz, W. D., 1978. *Double Stars* (Dordrecht: Reidel).

Henden, A. A., and Kaitchuck, R. H., 1982. *Astronomical Photometry* (New York: Reinhold).

Hynek, J. A., 1938. *Contr. Perkins Obs.*, No. 10.

Irwin, J. B., 1962, in *Astronomical Techniques*, W. A. Hiltner, ed. (Chicago: Chicago University Press).

Kopal, Z., 1959. *Close Binary Systems* (London: Chapman & Hall).

Lehmann–Filhes, R., 1894. *Astron. Nachr.* **134**, 89.

Lindemann, E. and Hauck, B., 1973. *Astron. Astrophys. Suppl.* **11**, 119.

McAlister, H. A., and Hartkopf, W. J., 1988. *Second Catalogue of Interferometric Measurements of Binary Stars*, Centre for High Angular Resolution Astronomy, Contr. No. 2 (Atlanta: CHARA, Georgia State University).

Mount Laguna Observatory, *Smith 24 inch Telescope Operating Manual*, Internal Publication, San Diego State University.

Oblak, E., Considère, S., and Chareton, M., 1976. *Astron. Astrophys. Suppl.* **24**, 69.

Petrie, R. M., 1962. *Pub. D. A. O.* **12**, 111.

Pickering, E. C., 1891. *Astron. Nachr.* **127**, 157.

Pike, C. D., 1978. *Mon. Not. Roy. Astron. Soc.* **184**, 265.

Russell, H. N., 1912. *Astrophys. J.* 35, 315.

Shajn, G., 1926. *Astron. Nachr.* **228**, 337.

Sterne, T. E., 1941. *Harvard Obs. Repr.* **222**.

Stickland, D. J., 1976. *Mon. Not. Roy. Astron. Soc.* **175**, 473.

Strömgren, B., 1963, in *Basic Astronomical Data*, ed. K. AA. Strand (Chicago: University of Chicago Press).

Tonry, J., and Davis, M., 1979. *Astron. J.* **84**, 1511.

Worley, C. E., 1967, in *On the Evolution of Double Stars*, ed. J. Dommanget, *Commun. Obs. Roy. Belgique*, Ser. B, No. 17.

Zeilik, M. and van Panhuys–Smith, E., 1987. *Introductory Astronomy and Astrophysics* 2nd. edition. (New York: CBS College Pub.), p. 239.

Appendix A

This Appendix was developed in the hope that it could be used as a "cook-book" in conjunction with the IRAF manuals and on–line help files, for reducing digitized spectra. It is assumed that the reader has used IRAF previously. If not, then a grasp of how the IRAF command language is set up may be attained by working through the IRAF beginner's manual. The following pages will describe the tasks necessary to reduce a spectrum and obtain a heliocentric radial velocity via cross–correlation. Task names and the packages in which they are found will be in bold face type, and the results of tasks have been illustrated by the use of plots wherever possible. A description of the steps taken to subtract a G spectrum from the composite spectrum has also been included.

Suppose we begin with images of the wedge calibration, the clear plate reading, an arc spectrum and a stellar spectrum. The first thing to realize is that the wedge image is not a one–dimensional image; there are ten lines which correspond to each calibration step (even though only one line at a time is plotted). Similarly, the PDS machine creates arc and stellar spectra each consisting of two lines (since these regions on the plate are scanned twice). In order to convert the arc and stellar spectra to one–dimensional spectra, the task **imcombine**, found in the package **images**, is used to average the two lines into one:

imcombine *arc image [* , 1] arc image [* , 2] arc image*

where the last file contains the combined image. The task may be used for the stellar spectrum as well.

The stellar spectra must be converted from a density to an intensity scale, prior to any subsequent reduction. The tasks necessary for this are found in the package **dtoi**. The first step in the conversion involves calculating the mean densities of the calibration wedges. Recall that there are ten lines in the required image; the calculation is performed using the task **spotlist**. For these purposes, the image files containing the wedges are supplied as:

wedge [, 1], wedge [* , 2], . . . , wedge [* , 10]*

The user also must specify the clear plate image (for calculation of the fog level, or clear plate reading) and the name of the output file (called a database, in IRAF). The next step matches the calibration density values to their corresponding log exposure times. There is a file containing the appropriate times for different combinations of emulsions and filters used at Kitt Peak; I found it necessary to create my own file patterned after the Kitt Peak file, but with my own exposure times and emulsion and filter type. By typing the task name **dematch** followed by the database name, the density values are assigned log exposure values. Now the task **hdfit** is implemented. This task plots the log of the exposure values against the log of the opacitance ($= log(10^{density} - 1)$ and fits a curve. The user may choose the type of polynomial to be fitted to the data. The resulting characteristic curve should look something like Figure A.1. The user should be aware of problems which may occur when performing this task. If the plate is underexposed, and since the clear plate density is subtracted from wedge densities before the curve is plotted, some new density values may be below zero. This results in nonsensical answers when the task tries to calculate the log opacitance values.

The omission of the faint wedge steps will allow the calculation of the characteristic curve, at the risk of losing part of the spectrum. Finally, one uses the task **hdtoi**, specifying the input and output image names, to apply the characteristic curve to the stellar spectrum. The fog level (which has been written to the database by the task **spotlist**) is automatically subtracted from the stellar image before transformation occurs.

Next, a wavelength scale is applied to the stellar images. The tasks required for this may all be found in the package **onedspec**. The task **identify** is used interactively with the combined arc image to assign wavelengths to individual features and obtain the dispersion curve. Note that this task has to be used only once; if the user has more than one arc image, the first dispersion curve may used to assign wavelengths to the other arcs using the task **reidentify** with the image whose features were initially identified. The dispersion curves are then applied to the stellar spectra, in the following manner. The user needs to specify which dispersion solution corresponds to which stellar image. By typing

refspectra *stellar image* reference = *arc image*

the name of the arc image is added to the stellar image's header. The solution is applied using **dispcor**. In this task, a starting and ending wavelength, the number of pixels, and the angstroms/pixel need to be specified. I specified the first three quantities; the fourth was found by the task. Note that the same number of pixels and angstroms/pixel should be assigned to each stellar image since the images must be exactly the same size for the cross–correlation to work. Finally, the stellar images are ready to be normalized. The task **continuum** flattens the spectra according to the method chosen by the user. The ratio method determines the ratio of the input spectrum to the fitted continuum, "fit" gives the fitted continuum spectrum and "difference" gives

Figure A.1: An example of a characteristic curve. A cubic spline polynomial was fit to the data.

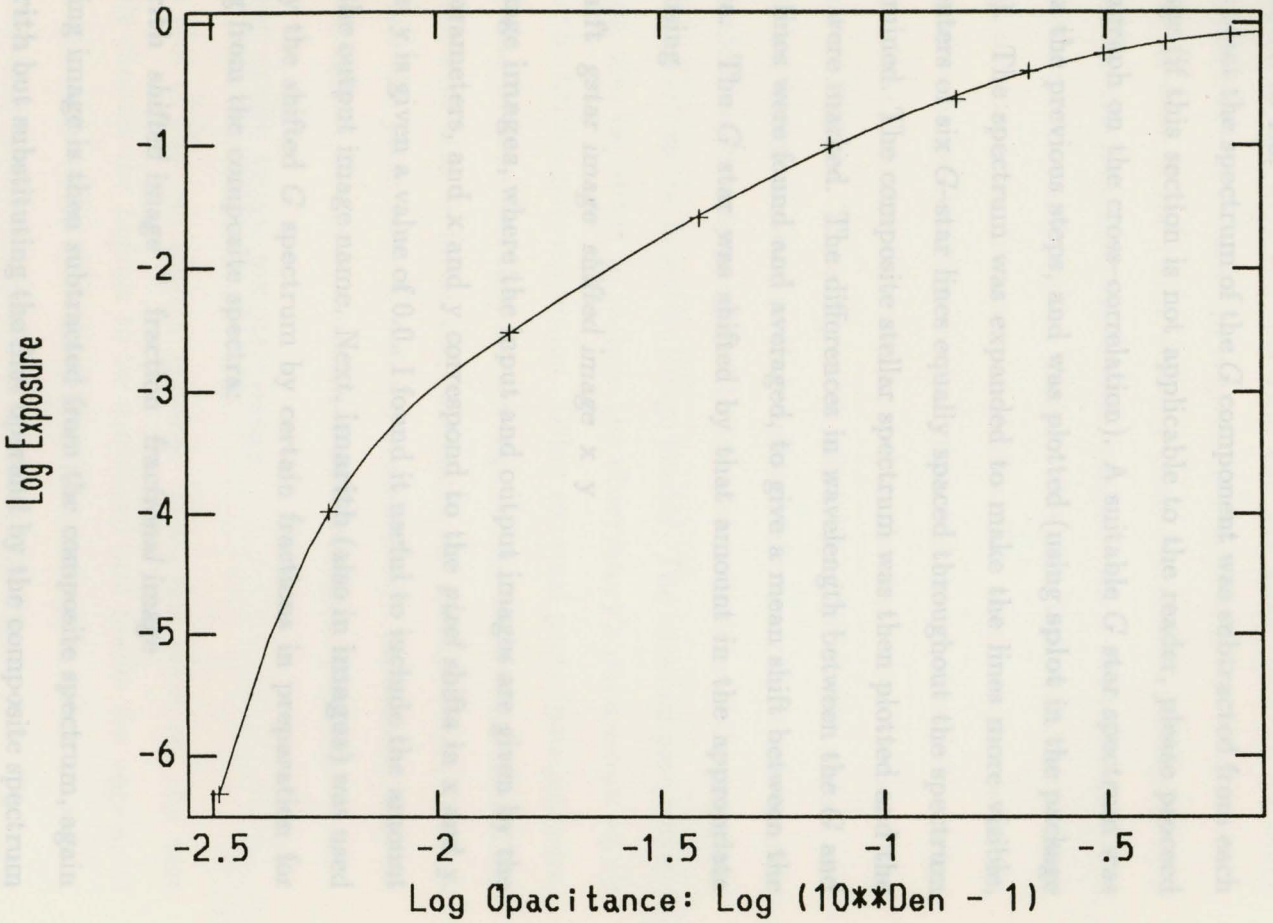

the difference between the input spectrum and the fitted continuum spectrum. I used a ratio method, whereby the output spectrum was flattened and normalized to 1.0.

At this point the spectrum of the *G* component was subtracted from each stellar image (if this section is not applicable to the reader, please proceed to the paragraph on the cross–correlation). A suitable *G* star spectrum was reduced via the previous steps, and was plotted (using **splot** in the package **onedspec**). The spectrum was expanded to make the lines more visible, and the centers of six *G*–star lines equally spaced throughout the spectrum were determined. The composite stellar spectrum was then plotted and the same lines were marked. The differences in wavelength between the *G* and composite lines were found and averaged, to give a mean shift between the two spectra. The *G* star was shifted by that amount in the appropriate direction, using

imshift *gstar image shifted image* x y

in the package **images**, where the input and output images are given by the first two parameters, and x and y correspond to the *pixel* shifts in x and y. In this case, y is given a value of 0.0. I found it useful to include the amount of shift in the output image name. Next, **imarith** (also in **images**) was used to multiply the shifted *G* spectrum by certain fractions in preparation for subtracting from the composite spectra:

imarith *shifted image* * fraction *fractional image*

The resulting image is then subtracted from the composite spectrum, again using **imarith** but substituting the first operand by the composite spectrum image, the operator by – and the second operand by *fractional image*, and supplying a new name for the output image. I had an idea of how much

should be subtracted; various fractions of the G spectrum were subtracted and the resulting stellar images were plotted to see which fraction was correct. An example of an unsubtracted spectrum and the same spectrum in which the correct amount was subtracted is given in Figure A.2.

The task **rvxcor** in the radial velocity cross–correlation package (**rv**) is used to obtain velocities from the stellar images. Since the task computes heliocentric corrections and applies them to the observed velocities, several things must be done prior to cross–correlation. The external parameter set (hereafter known as pset) **rvkeywords** contains all the required information pertaining to the particular observation, such as the star's coordinates, times of exposure, and so on. These keywords must be added to the object and template stellar image headers so that heliocentric corrections can be performed. In addition, the observed and heliocentric velocities of the template star must be added to the template image header. The external pset **observatory** must also be edited to include the observatory's parameters which are used in the heliocentric correction. Other external psets (**processpars**, **filterpars**) may be used, but they are not required for basic cross–correlating techniques. It may also be favourable to smooth the spectra before the correlation, since the plate noise is reduced considerably. Smoothing may be done while in **splot**. The cross–correlation task is begun by typing

rvxcor *stellar image template image*

whereby a plot of the two spectra appears. From this point on, the user interactively chooses the regions to be correlated and marks the regions of the correlation peak to be fit. To begin, the user types :cont to refit a continuum to each spectrum, resulting in a plot like Figure A.3. The user may now type an x to start the cross–correlation, or mark regions (using g) to be used in the correlation. I found it helpful to only use the lines and

Figure A.2: The first spectrum is a representative spectrum of α Equulei. The second has had 10 percent of the G star subtracted, which was determined to be the correct amount for this particular plate. For comparison, 68 Tauri's spectrum has been included.

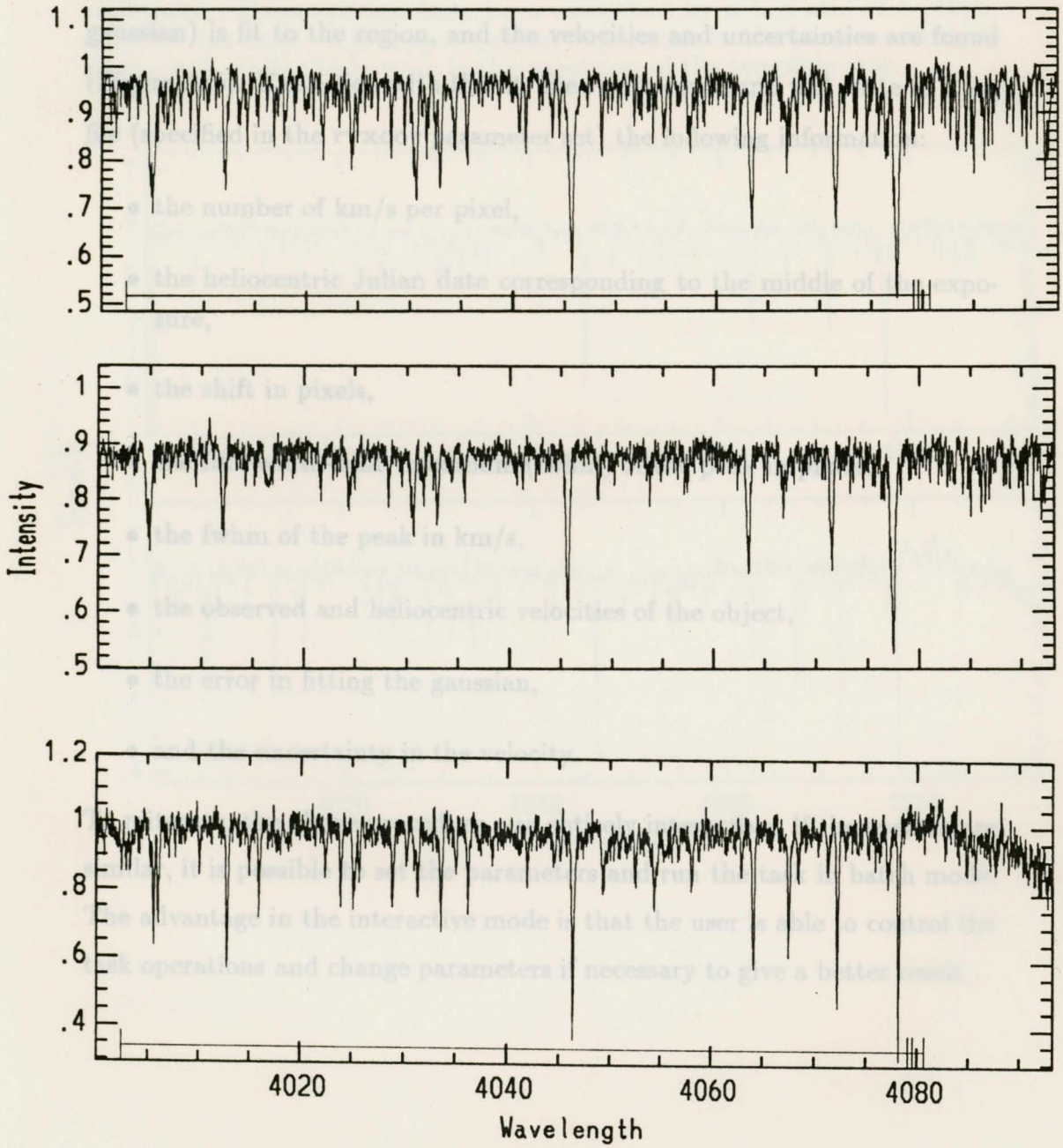

not the surrounding continuum, since some spectra were noisy (even after smoothing) and omission of as much of the continuum as possible increased the signal. The correlation gives a plot of the correlation function, similar to Figure A.4. A region of the curve is selected, a function (parabolic or gaussian) is fit to the region, and the velocities and uncertainties are found (Figure A.5). If satisfied with the fit, the :write command will write to a log file (specified in the **rvxcor** parameter set) the following information:

- the number of km/s per pixel,
- the heliocentric Julian date corresponding to the middle of the exposure,
- the shift in pixels,
- the full–width–half–maximum (fwhm) of the peak in pixels,
- the fwhm of the peak in km/s,
- the observed and heliocentric velocities of the object,
- the error in fitting the gaussian,
- and the uncertainty in the velocity.

To reiterate, the above procedure was entirely interactive. If the spectra are similar, it is possible to set the parameters and run the task in batch mode. The advantage in the interactive mode is that the user is able to control the task operations and change parameters if necessary to give a better result.

Figure A.3: Continuum normalized spectra before the cross–correlation is performed. These spectra have been smoothed by a box size of 5 pixels prior to this task. The upper (object) spectrum is the same as that in Figure A.2, while the bottom is the spectrum of the template star.

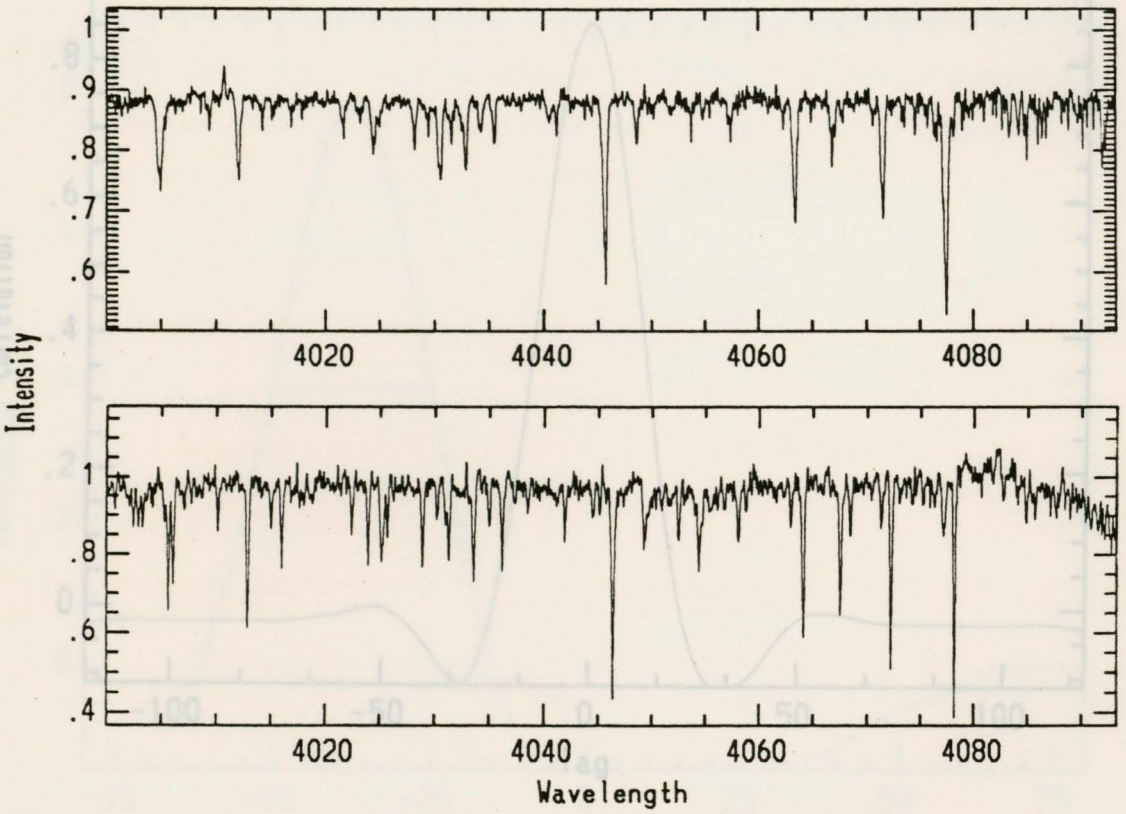

Figure A.4: The correlation function displayed after typing x. Note the high correlation. Lag is given in pixels.

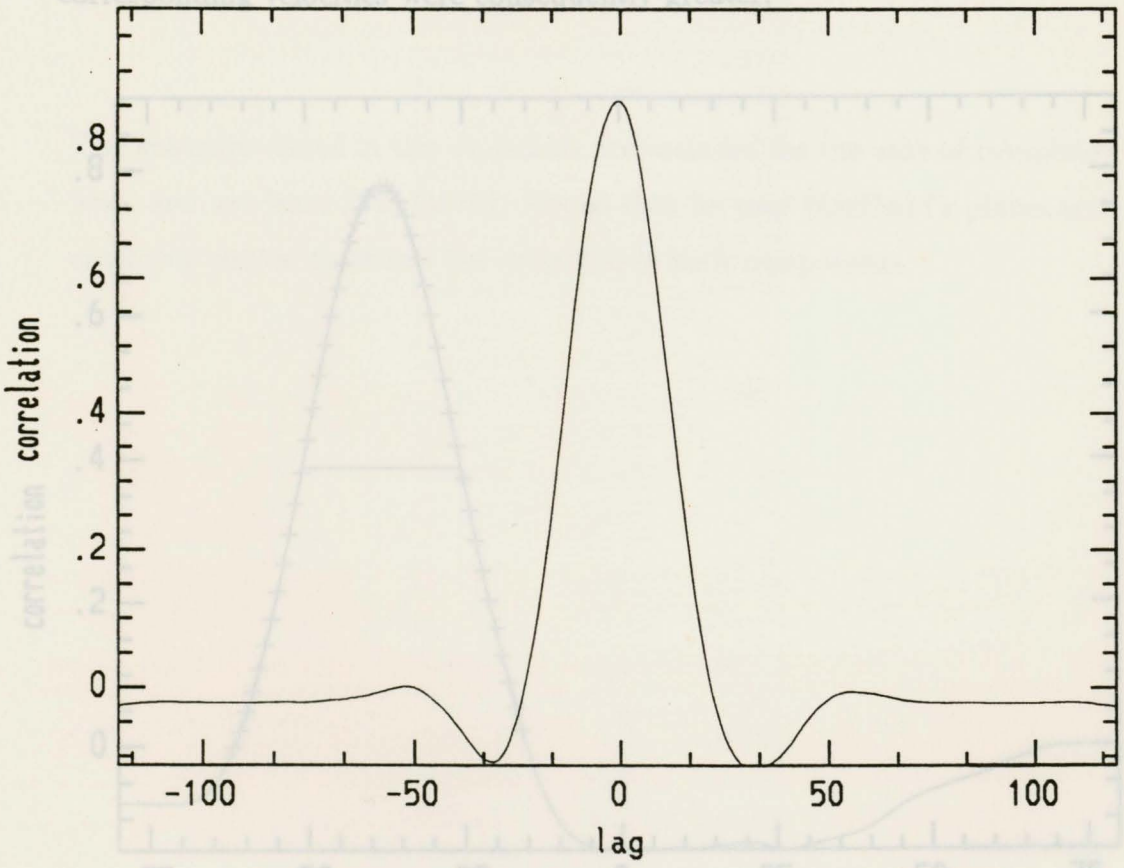

Note: The conversion factor from pixels to velocity units (ie. km/s) is 1.3166 km/s per pixel.

Figure A.5: Another example of the correlation function, marked and fit with a gaussian. Not all spectra were of good quality, hence some correlation functions were not as high or narrow as others. The errors in their corresponding velocities were consequently greater.

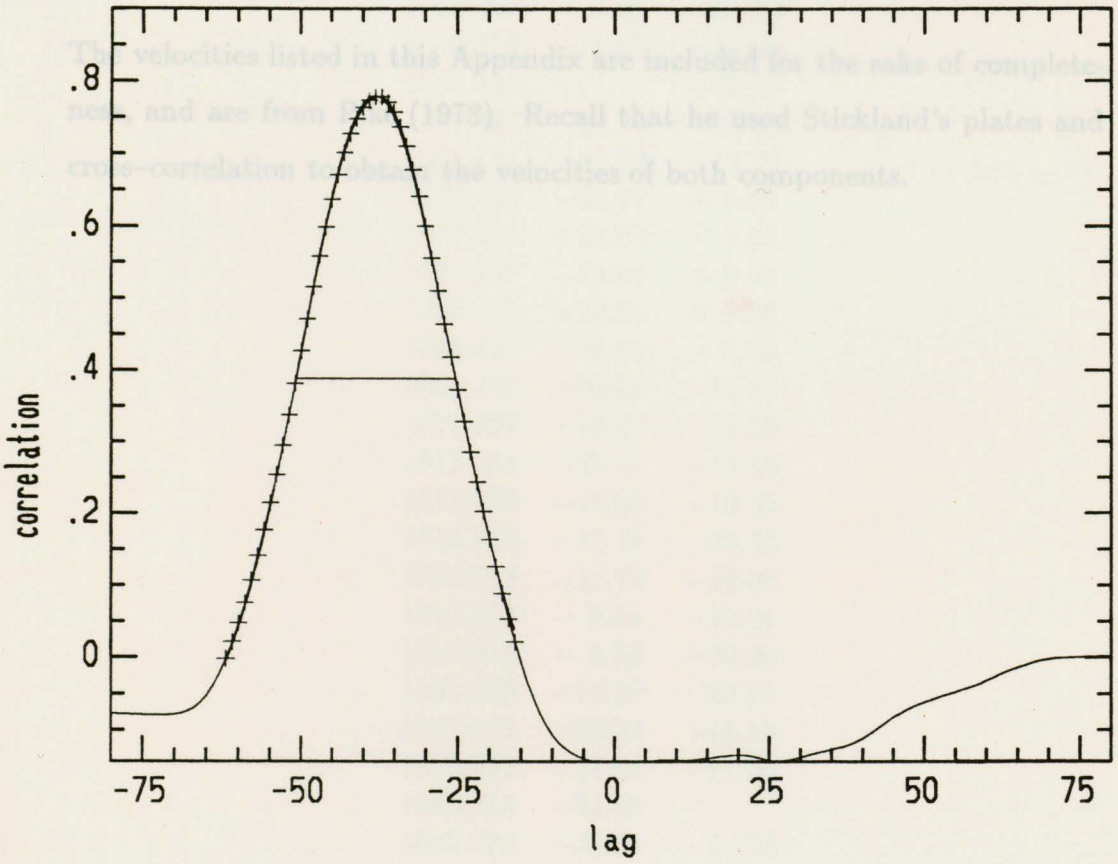

Appendix B

The velocities listed in this Appendix are included for the sake of completeness, and are from Pike (1978). Recall that he used Stickland's plates and cross–correlation to obtain the velocities of both components.

Table B.1: Pike's (1978) velocities of α Equulei.

HJD 2440000+	V_G km/s	V_A km/s
1510.590		−16.70
1513.597		−22.60
1538.497	− 1.90	−35.70
1540.519	− 1.85	−41.90
1553.427		−29.80
1566.427	−20.90	−13.80
1567.434	−21.02	−12.80
1587.455	−33.77	+ 0.60
1597.326	−28.08	− 1.50
1599.292	−29.03	+ 0.50
1606.375	−23.90	− 7.60
1606.425	−24.81	− 8.60
1608.276	−23.69	−14.90
1611.323	−19.87	−15.50
1612.354	−20.77	−16.90
1615.320	−16.62	−19.30
1616.264	−12.79	−23.50
1623.313	−12.79	−22.80
1643.219	− 3.44	−37.00
1645.215	− 5.58	−39.40
1655.233	−12.92	−28.90
1667.215	−23.52	−15.10
1670.222	−26.20	−14.20
1682.215	−34.56	
1683.222	−35.60	− 0.705
1980.285	−34.96	+ 1.00
1993.224	−31.00	− 0.40
2004.220	−24.18	−16.50
2007.235		−13.90
2016.205	−13.05	−27.30
2026.217		−33.4

Appendix C

This Appendix contains the photometric data which were used in the analysis of 20 Leonis. The data have been partially reduced; time is expressed as Julian date, and photon counts in each filter have been reduced to differential magnitudes, in the sense *variable – comparison.*

Table C.1: Photometric data for 20 Leonis.

JD 2440000+	Δy	Δb	Δv	Δu
7568.8041	−1.304	−1.450	−1.532	−1.150
7568.8136	−1.295	−1.441	−1.520	−1.128
7568.8667	−1.303	−1.466	−1.553	−1.159
7568.8793	−1.295	−1.438	−1.520	−1.117
7568.8876	−1.297	−1.431	−1.503	−1.117
7568.8958	−1.297	−1.436	−1.506	−1.117
7568.9059	−1.271	−1.417	−1.502	−1.113
7568.9158	−1.264	−1.413	−1.498	−1.110
7568.9246	−1.290	−1.433	−1.519	−1.140
7568.9367	−1.310	−1.440	−1.509	−1.121
7568.9444	−1.310	−1.456	−1.546	−1.148
7568.9525	−1.304	−1.449	−1.527	−1.142
7568.9634	−1.295	−1.441	−1.528	−1.130
7568.9744	−1.261	−1.410	−1.498	−1.096
7568.9916	−1.285	−1.418	−1.485	−1.103
7569.7114	−1.309	−1.461	−1.545	−1.146
7569.7192	−1.300	−1.452	−1.545	−1.132
7569.7280	−1.293	−1.451	−1.539	−1.148
7569.7359	−1.280	−1.424	−1.505	−1.117
7569.7433	−1.301	−1.448	−1.529	−1.144
7569.7522	−1.292	−1.440	−1.519	−1.125
7569.7590	−1.280	−1.436	−1.521	−1.131
7569.7654	−1.292	−1.446	−1.528	−1.142
7569.7752	−1.313	−1.465	−1.554	−1.149
7569.7823	−1.309	−1.474	−1.564	−1.167
7569.7888	−1.291	−1.446	−1.535	−1.125
7569.8707	−1.313	−1.468	−1.565	−1.174
7569.8789	−1.297	−1.460	−1.543	−1.156
7569.8859	−1.297	−1.450	−1.531	−1.136
7569.8952	−1.302	−1.442	−1.524	−1.131
7569.9025	−1.272	−1.413	−1.492	−1.087

Table C.1, continued.

JD 2440000+	Δy	Δb	Δv	Δu
7569.9098	−1.277	−1.430	−1.507	−1.115
7569.9181	−1.287	−1.436	−1.522	−1.120
7569.9249	−1.295	−1.447	−1.537	−1.140
7569.9316	−1.313	−1.460	−1.539	−1.138
7569.9395	−1.326	−1.466	−1.549	−1.148
7569.9476	−1.321	−1.476	−1.558	−1.168
7569.9552	−1.316	−1.469	−1.552	−1.158
7569.9638	−1.330	−1.478	−1.559	−1.160
7569.9706	−1.319	−1.459	−1.542	−1.130
7569.9781	−1.286	−1.432	−1.513	−1.106
7570.8851	−1.293	−1.426	−1.505	−1.121
7570.8925	−1.286	−1.424	−1.513	−1.109
7570.9022	−1.274	−1.417	−1.492	−1.102
7570.9094	−1.267	−1.415	−1.495	−1.116
7570.9198	−1.265	−1.412	−1.500	−1.124
7570.9286	−1.293	−1.440	−1.527	−1.135
7570.9368	−1.296	−1.443	−1.525	−1.137
7570.9477	−1.314	−1.464	−1.528	−1.145
7570.9560	−1.298	−1.445	−1.525	−1.125
7570.9654	−1.276	−1.411	−1.491	−1.093
7570.9758	−1.297	−1.431	−1.504	−1.106
7570.9843	−1.263	−1.421	−1.504	−1.115
7570.9950	−1.290	−1.416	−1.500	−1.108
7571.0027	−1.288	−1.422	−1.497	−1.115
7571.0101	−1.272	−1.426	−1.502	−1.108
7572.6652	−1.304	−1.459	−1.534	−1.144
7572.6735	−1.300	−1.425	−1.484	−1.092
7572.6840	−1.300	−1.446	−1.525	−1.148
7572.6919	−1.302	−1.447	−1.529	−1.148
7572.6996	−1.275	−1.417	−1.497	−1.102
7572.7094	−1.278	−1.424	−1.502	−1.135

Table C.1, continued.

JD 2440000+	Δy	Δb	Δv	Δu
7572.7168	−1.287	−1.436	−1.515	−1.124
7572.7247	−1.281	−1.428	−1.506	−1.119
7572.7329	−1.282	−1.430	−1.512	−1.139
7572.7397	−1.285	−1.438	−1.519	−1.135
7572.7478	−1.288	−1.436	−1.529	−1.136
7572.7538	−1.294	−1.434	−1.516	−1.118
7572.7615	−1.292	−1.437	−1.529	−1.134
7572.7696	−1.299	−1.449	−1.539	−1.139
7572.7762	−1.299	−1.446	−1.524	−1.135
7572.7826	−1.278	−1.434	−1.512	−1.132
7572.7898	−1.266	−1.409	−1.492	−1.100
7572.7970	−1.285	−1.437	−1.512	−1.126
7572.8027	−1.282	−1.429	−1.508	−1.120
7572.8105	−1.277	−1.434	−1.517	−1.130
7572.8158	−1.280	−1.439	−1.537	−1.141
7572.8212	−1.281	−1.434	−1.531	−1.130
7572.8691	−1.293	−1.434	−1.515	−1.125
7572.8763	−1.296	−1.430	−1.517	−1.112
7572.8824	−1.299	−1.439	−1.519	−1.126
7572.8901	−1.281	−1.422	−1.501	−1.102
7572.8959	−1.295	−1.447	−1.522	−1.135
7572.9016	−1.297	−1.451	−1.525	−1.141
7572.9113	−1.297	−1.448	−1.527	−1.133
7572.9173	−1.294	−1.455	−1.544	−1.137
7572.9234	−1.290	−1.444	−1.526	−1.127
7572.9312	−1.301	−1.452	−1.528	−1.145
7572.9383	−1.292	−1.443	−1.520	−1.129
7572.9451	−1.258	−1.420	−1.498	−1.113
7572.9538	−1.285	−1.429	−1.510	−1.124
7572.9618	−1.278	−1.432	−1.520	−1.127
7572.9694	−1.276	−1.434	−1.515	−1.129

Table C.1, continued.

JD 2440000+	Δy	Δb	Δv	Δu
7572.9784	−1.273	−1.427	−1.500	−1.124
7572.9852	−1.269	−1.420	−1.506	−1.115
7572.9913	−1.295	−1.442	−1.512	−1.119
7573.6759	−1.316	−1.477	−1.560	−1.165
7573.6818	−1.315	−1.467	−1.550	−1.157
7573.6890	−1.297	−1.448	−1.532	−1.140
7573.6953	−1.292	−1.444	−1.523	−1.114
7573.7020	−1.297	−1.454	−1.536	−1.131
7573.7090	−1.293	−1.453	−1.539	−1.154
7573.7157	−1.289	−1.437	−1.529	−1.138
7573.7227	−1.285	−1.425	−1.515	−1.109
7573.7285	−1.288	−1.440	−1.522	−1.133
7573.7363	−1.298	−1.453	−1.527	−1.143
7573.7420	−1.309	−1.456	−1.538	−1.143
7573.7500	−1.301	−1.447	−1.524	−1.123
7573.7575	−1.303	−1.459	−1.542	−1.145
7573.7645	−1.298	−1.456	−1.541	−1.145
7573.7703	−1.303	−1.454	−1.521	−1.119
7573.7780	−1.296	−1.448	−1.539	−1.127
7573.7846	−1.294	−1.438	−1.526	−1.134
7573.7919	−1.290	−1.435	−1.522	−1.121
7573.7984	−1.297	−1.452	−1.530	−1.138
7573.8080	−1.285	−1.449	−1.539	−1.152
7573.8182	−1.316	−1.455	−1.516	−1.113
7573.8268	−1.307	−1.449	−1.529	−1.124
7573.8340	−1.308	−1.451	−1.529	−1.138
7574.8243	−1.293	−1.443	−1.524	−1.131
7574.8294	−1.293	−1.440	−1.527	−1.125
7574.8360	−1.290	−1.438	−1.521	−1.130
7574.8414	−1.289	−1.434	−1.525	−1.133
7574.8511	−1.280	−1.427	−1.509	−1.120

Table C.1, continued.

JD 2440000+	Δy	Δb	Δv	Δu
7574.8578	−1.267	−1.416	−1.508	−1.117
7574.8644	−1.274	−1.425	−1.507	−1.121
7574.8696	−1.295	−1.439	−1.508	−1.122
7574.8777	−1.281	−1.437	−1.516	−1.116
7574.8829	−1.288	−1.437	−1.513	−1.115
7574.8899	−1.291	−1.437	−1.516	−1.132
7574.8949	−1.283	−1.433	−1.514	−1.129
7574.9012	−1.281	−1.437	−1.521	−1.126
7574.9076	−1.293	−1.441	−1.515	−1.113
7574.9138	−1.293	−1.444	−1.530	−1.132
7574.9192	−1.283	−1.428	−1.516	−1.122
7574.9421	−1.279	−1.425	−1.502	−1.131
7574.9481	−1.264	−1.414	−1.496	−1.112
7574.9554	−1.273	−1.415	−1.497	−1.111
7574.9614	−1.286	−1.435	−1.508	−1.113
7574.9686	−1.281	−1.432	−1.514	−1.124
7574.9746	−1.283	−1.428	−1.514	−1.136
7574.9824	−1.285	−1.435	−1.515	−1.125
7574.9884	−1.288	−1.441	−1.526	−1.117
7574.9957	−1.295	−1.443	−1.529	−1.139
7575.0013	−1.279	−1.442	−1.520	−1.144

Vita

Surname: **Rosvick (née Baer)** Given Names: **Joanne Marie**

Place of Birth: **Edmonton, Alberta**

Date of Birth: **April 30, 1965**

Educational Institutions Attended:

University of Alberta, Edmonton	**1983 to 1987**
University of Victoria, Victoria	**1988 to 1990**

Degrees Awarded:

B. Sc. (Specialization) 1987	**University of Alberta**

Honors and Awards:

Rutherford Heritage Scholarship	**1983-84**
Department of Physics Book Prize	**1985**
Samuel J. McCoppen Bursary	**1985-86**
J. A. Jacobs Prize in Physics	**1987**

Partial Copyright License

I hereby grant the right to lend my thesis (the title of which is shown below) to users of the University of Victoria Library, and to make single copies only for such users, or in response to a request from the library of any other university or similar institution, on its behalf or for one of its users. I further agree that permission for extensive copying of this thesis for scholarly purposes may be granted by me or a member of the university designated by me. It is understood that copying or publication of this thesis for financial gain shall not be allowed without my written permission.

Title of Thesis:

A Study of Two Spectroscopic Binary Systems

[redacted]

Author: Rosvick, Joanne Marie

October 31, 1990